SIGNAL STATISTICS OF PHASE DEPENDENT OPTICAL TIME DOMAIN REFLECTOMETRY

A Dissertation

by

ALEKSANDER KAROL WÓJCIK

Submitted to the Office of Graduate Studies of
Texas A&M University
in partial fulfillment of the requirements for the degree of

DOCTOR OF PHILOSOPHY

December 2006

Major Subject: Electrical Engineering

SIGNAL STATISTICS OF PHASE DEPENDENT OPTICAL TIME DOMAIN REFLECTOMETRY

A Dissertation

by

ALEKSANDER KAROL WÓJCIK

Submitted to the Office of Graduate Studies of
Texas A&M University
in partial fulfillment of the requirements for the degree of

DOCTOR OF PHILOSOPHY

Approved by:

Co-Chairs of Committee,	Chin B. Su
	Henry F. Taylor
Committee Members,	Robert D. Nevels
	Steven D. Taliaferro
Head of Department,	Costas Georghiades

December 2006

Major Subject: Electrical Engineering

ABSTRACT

Signal Statistics of Phase Dependent

Optical Time Domain Reflectometry. (December 2006)

Aleksander K. Wójcik, B.S., Instituto Tecnológico

y de Estudios Superiores de Monterrey;

M.Eng., Texas A&M University

Co–Chairs of Advisory Committee: Dr. Chin B. Su
Dr. Henry F. Taylor

The statistics of the phase dependent optical time-domain reflectometer have been analyzed. The optical fiber is modeled by the use of a discrete set of reflectors positioned randomly along the fiber. The statistics of the reflected light from a traveling pulse are derived. The statistics of the signal are used to calculate the characteristics of shot noise in the photodetector, and the probability that noise of certain intensity will occur. An estimation of the backscattered power is made by calculating the fraction of the backscattered power that is captured in a guiding mode. Upper power limits are calculated by considering nonlinear optical effects. An estimation of noise from thermally excited sound waves, amplified by Brillouin scattering, is derived. This noise considers the parameters of a photodetector, giving a model for the noise in the measurable photocurrent. Two models are used to describe the fading probability of the signal. The first model, based on the Fabry-Perot interferometer with a random phase perturbation in the middle, is used to calculate the probability that the whole signal vanishes for any value of phase perturbation. The second model, by calculating the correlation between two signals, one perturbed and one unperturbed, predicts the fading of the signal of interest. The present work gives the theoretical basis for the phase dependant Optical Time Domain Reflectometry, allowing its optimization and setting the fundamental limitations to the performance

of the system.

To the Memory of My Father and My Family

ACKNOWLEDGMENTS

I want to express my gratitude to Dr. Chin Su for his help and guidance. I want to thank him for giving me the opportunity to successfully finish my studies.

Special thanks go to the late Dr. Henry Taylor for his support and guidance during my research work. His deep knowledge of the field, generosity and hard work will always have my respect and admiration.

I would also like to thank Dr. Robert Nevels and Dr. Steven Taliaferro for volunteering their time and effort as my committee members and their comments and suggestions on my work. I want to extend my gratitude to Dr. Krzysztof Michalski and Dr. Dante DeBlassie for their continuous help and their patience for my never ending questions.

I want to especially thank my parents, my mother, Mrs. Jadwiga Wójcik, and my father, the late Dr. Aleksander Wójcik, for their unconditional love and support. They have encouraged me through my whole life and gave me the motivation and energy to do this work. They taught me about kindness, honor and love, but also about science and philosophy. I'm very grateful to my sister and her husband, Dr. Ewa Wójcik and Dr. Alejandro Oliver; they have always supported me and helped me in everything they could.

I also want to thank my dear friend, Dr. Bei Xu, for the detailed reading of the manuscript.

TABLE OF CONTENTS

CHAPTER Page

LIST OF TABLES

LIST OF FIGURES

FIGURE Page

CHAPTER I

INTRODUCTION

A. Background

The optical time domain reflectometer (OTDR) has been used for decades to characterize anomalies in optical fiber links [1]. Its extension to single mode fibers followed few years later [2]. The principle behind OTDR is the Rayleigh scattering phenomena. The natural density fluctuations, present in non-crystalline (amorphous) homogenous materials, translate into local variations of permittivity of the material [3]. Light propagating inside such medium will be scattered in all directions. The original theory was derived to explain the blue color of the sky, and it has been confirmed experimentally [4]. The same ideas have been successfully applied to explain scattering phenomena in glasses, giving quantitative estimates from thermodynamical arguments [5, 6]. The glass is treated as a liquid with extremely high viscosity. The model requires the use of the concept of fictive temperature, being this the temperature at which the glass solidifies.

Recent theoretical and experimental advances permitted better understanding of the phenomena of propagation of light in the fiber, such as nonlinear effects and propagation of sound waves. This combined with the development of optical fiber technology, and new kinds of lasers, allowed the applications of fiber optics in sensors [7, 8, 9], for example as a fiber optic gyroscope [10], in biology [11] and automobile industry [12].

OTDRs are commonly used as part of the fiber sensors. They permit the analysis of local effects on the light inside the fiber, by the analysis of the signal at one of the

---

The journal model is *IEEE Journal of Lightwave Technology.*

ends. This makes possible to construct distributed sensors. The special geometry of the fiber makes it particularly suited for long range distributed sensors.

Rayleigh backscattering consists of the addition of large number of signals from microscopic scatterers. A common problem with systems where a large number of interfering signals contribute to the signal of interest is the fading phenomena. This problem has been widely studied in the mobile communications context [13]. Fading is present in coherent OTDR systems as well, and can affect the performance of the system. Several experimental techniques have been implemented to analyze and possibly minimize this effect [14, 15, 16, 17].

B. Experiment

In an OTDR, laser pulses are launched into the fiber and the returned signal is analyzed in time domain. A modified version of OTDR has been developed at Texas A&M University to detect and locate time dependent phase variations along the fiber. This technique uses a very stable (low frequency drift) and narrow linewidth, single mode laser source. The use of a highly coherent laser is known as coherent OTDR (C-OTDR) or phase-sensitive OTDR (ϕ-OTDR) [18]. The main difference between C-OTDR and ϕ-OTDR is the use of heterodyne detection in the former and direct detection in the latter. The use of this kind of source presents a considerable modification to the traditional OTDR, where the coherent effects, fundamental for ϕ-OTDR, are considered undesirable noise known as Coherent Rayleigh Noise (CRN) [19, 20]. The backscattered signal is sensed using a photodetector and then analyzed. The coherent addition of the amplitudes of light waves scattered from spatially distributed centers makes it highly sensitive to variations of phase inside the fiber [21].

The ϕ-OTDR intrusion sensor system consists of a continuous wave laser, mod-

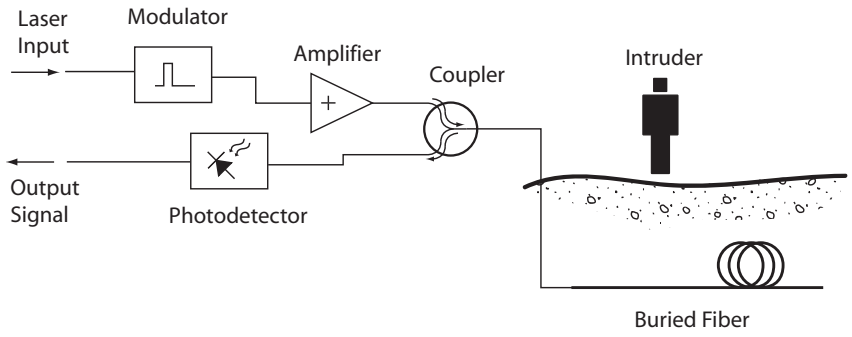

Fig. 1. Intrusion sensor system.

ulated in form of pulses, amplified by an erbium doped amplifier and launched into the fiber. The backscattered light is coupled to a photodetector and analyzed using a computer, as shown on Fig. 1. When an intruder steps over the fiber, induces a variation of pressure with time, at a particular location along the fiber.

The linewidth of the laser is vital for this application, since coherence time is of the order of the inverse of the bandwidth of the light [22],

$$\Delta t \sim \frac{1}{\Delta \nu}. \tag{1.1}$$

It was necessary to build a laser with a very narrow bandwidth and low frequency drift. The laser consists of a 980 nm laser diode, used as a pump laser, coupled into 3m long, Er^{3+} doped fiber (7 dB/m gain) through a wavelength division multiplexing (WDM) coupler. The resonant laser cavity is built by two fiber Bragg gratings (FBG), one of 99.9% reflectance on the backside and the other one of 92% reflectance on the output side [18]. The laser operates in a single mode, with a wavelength of 1555.4 nm, its linewidth is 3 kHz, the output power is 50μW. Its frequency drift, depending on ambient temperature, is of the order of 1 MHz/min [23]. The light is then amplified and modulated in amplitude, in form of pulses, by an optical modulator.

The laboratory tests of the whole system were performed by simulating the effect

of an intruder by a phase modulator. The modulator was constructed by wrapping 10 m of fiber around a piezoelectric (PZT) cylinder. The PZT section was in between two spools of fiber, of 2 km and 10 km long respectively. The results of these tests demonstrated that the signal pulses applied to PZT modified the OTDR signal noticeably, making possible to detect phase changes located 42 km away from the source [24].

The system has been demonstrated in two field tests, where a length of fiber was buried and a person walked on the ground above it. This produced a phase perturbation, and the intruder was detected by the sensor. The signal at the receiver was separated into two orthogonal polarizations, each one of them detected separately. For the field tests, the source signal had to be amplified. The first test used an 8.5 km length of cable buried 30 cm deep. The cable contained two fibers, spliced together at the far end to form a loop. A 2 km spool of fiber connected the monitoring equipment to one of the fibers in the buried cable. The operation of the system is illustrated by Fig. 2, where the spectral characteristics of the output have been measured.

The system was able to detect people walking over and near the fiber, as well as a car driving near it, proving its potential [23], and motivating further theoretical analysis of the ϕ-OTDR.

C. Contribution

This dissertation analyzes the statistical properties of the signal of interest in ϕ-OTDR. It covers the aspects of power limitations of the signal, probability of fading, correlation of perturbed and unperturbed signals and shot noise. Chapter II describes a general overview of the propagation of the pulse signal inside the fiber.In Chapter III a Fabry-Perot model of the ϕ-OTDR is introduced. The model is used to analyze

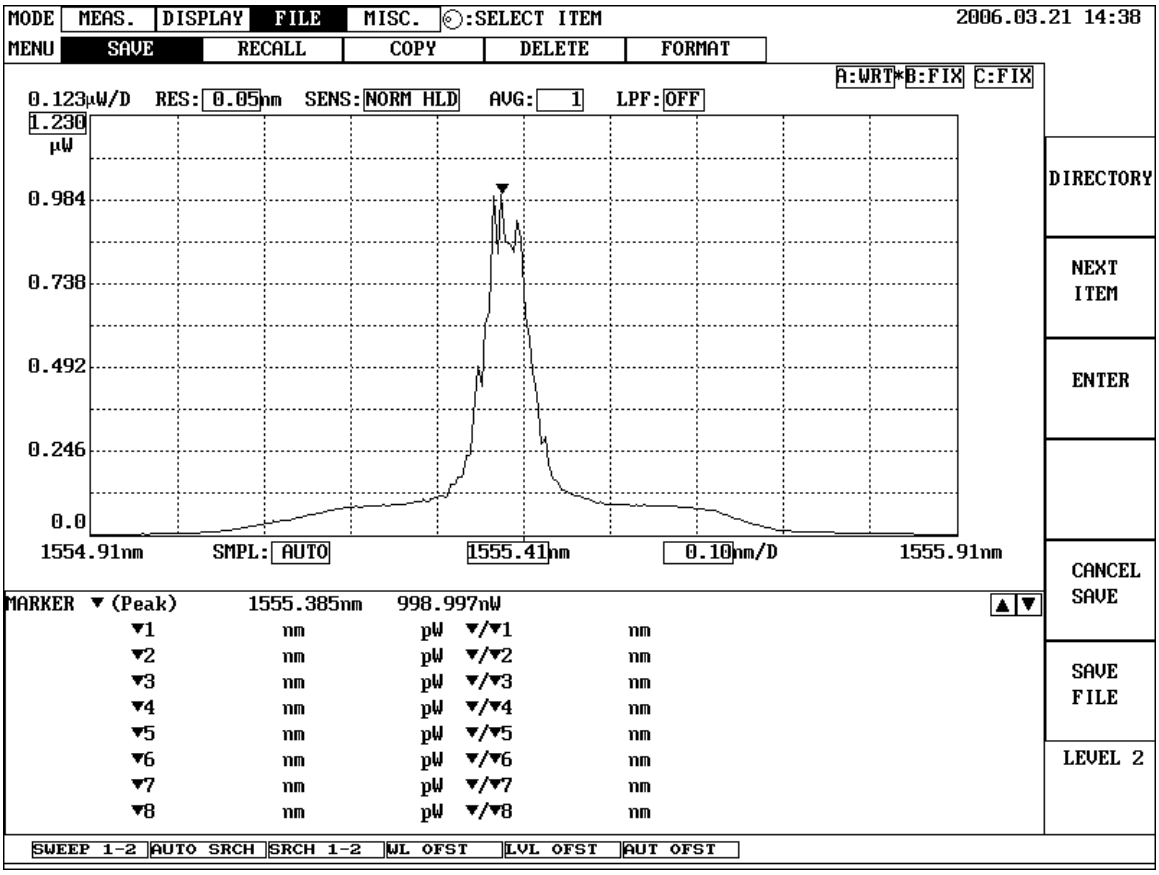

Fig. 2. Spectrum of the backscattered signal.

two kinds of fading effects in the system. The probability of fading of the signal is calculated, and a Monte Carlo simulation is performed. In Chapter IV the correlation between a perturbed and unperturbed signal is calculated, for arbitrary phase of perturbation and its position in the pulse. The result is used to calculate the probability distribution function of the output signal, with and without losses in the fiber. Chapter V deals with the shot noise, unavoidable in any optical system. In this chapter the probability that the noise exceeds an arbitrary threshold is derived. Chapter VI covers the upper limits of power and pulse length imposed by Brillouin nonlinear effects. Brillouin scattering is analyzed also as source of noise, taking into account the characteristics of the photodetector. Chapter VII gives a quantitative

estimation of power levels expected at the receiver, from the Rayleigh backscattering theory point of view. A comparison between the presented geometrical optics approach and Lorentz reciprocity theorem approach for a step index fiber is made in order to validate the model. The number of photons is calculated, which in view of the large number of photons involved, discards the necessity of quantum theory.

CHAPTER II

PROPAGATION IN THE OPTICAL FIBER

A. Modeling of Rayleigh Scattering

An optical fiber is not perfectly homogenous and has microscopic density fluctuations, as shown in Fig. 3a. The light launched into the fiber will be scattered in all directions. The backscattered light in the fiber exhibits the characteristics of Rayleigh scattering, which implies that the size of the fluctuation densities must be much smaller than the wavelength of the laser light λ. Part of that light, will be captured by a guided mode and propagate in the reverse direction. The number of such microscopic scatterers is very large and a statistical model has been proposed [25], where the scatterers are represented as randomly distributed reflectors, as shown in Fig. 3b. If we consider discrete time increments Δt, and take v_g as the speed of propagation of the pulse, we can define Δz as a minimum resolution length of the model. For our purposes it is possible to use the LP approximation [26] of the modes inside the fiber, and model the ϕ-OTDR in one dimension. This reduces the problem into a series of reflectors, as shown in Fig. 3c.

B. Propagation of a Light Pulse in a Fiber

As the light propagates inside the fiber, using the model defined above, some of the reflectors will be excited. The excited reflectors will change as the pulse propagates in time. This is shown on Fig. 4. In Fig. 4a the pulse is at time t_1 and then it travels inside the fiber, and at time t_2 another set of reflectors is excited. We can see that the signal from more than one reflector will be excited during an overlapping period of time. During this period, the reflected signals from both scatterers will arrive at

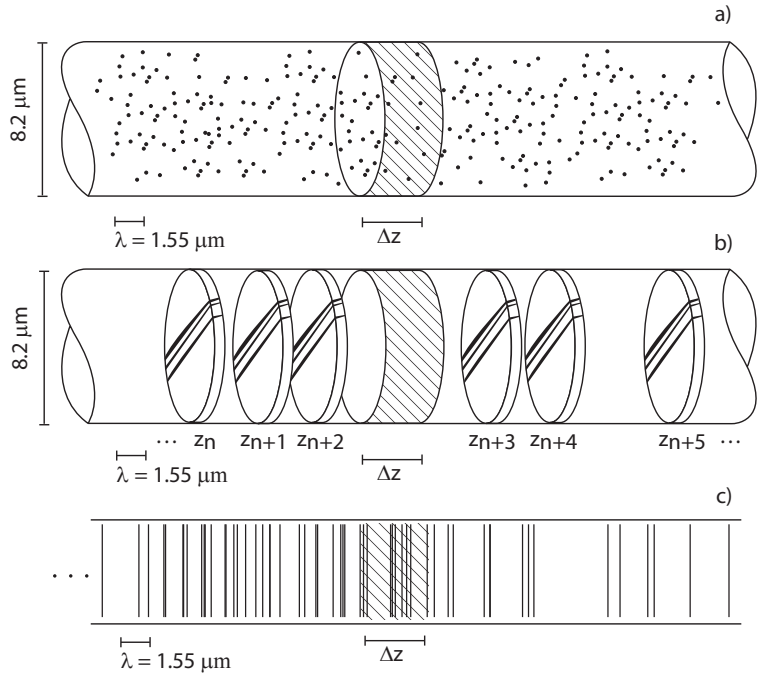

Fig. 3. Equivalent model of density fluctuations. a) Density fluctuations in the fiber. b) Equivalent model with density fluctuations replaced by reflectors. c) Simulation model of randomly distributed reflectors.

the same time at the origin, and will interfere with each other.

In the $\phi - OTDR$, a pulse of highly coherent light is injected into a fiber, and a phase shift representing the signal of interest is applied at some point along the fiber. Fig. 5 illustrates the relation between time delay and the location of a light pulse in a fiber. The leading edge of the pulse entered the fiber at $z = 0$ at time $t = 0$, and reached the location at which a phase shift is applied at time $t = T$. The trailing edge of the pulse passed that same location at a time $T + \Delta t$, with Δt the temporal width of the pulse. The time at which the backscattered light passed out of the fiber at $z = 0$ is denoted by $t*$. The solid triangles indicate the location in the fiber for which the backscattered light exited the fiber at a particular value of $t* : \tau_1 = 2T + \Delta t/2$ for the left set of pulses, and $\tau_2 = 2T + \Delta t/4$ for the right set. It is evident from these

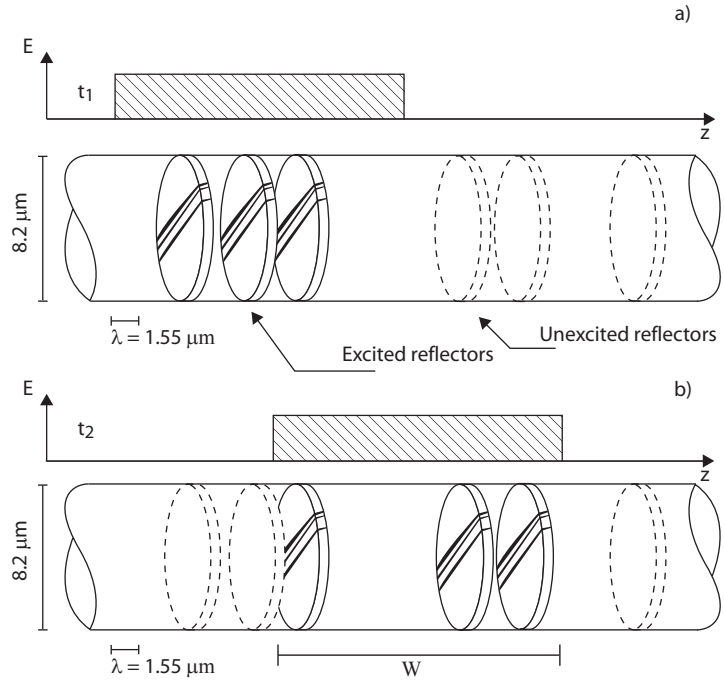

Fig. 4. Pulse traveling inside the fiber. a) The pulse in the fiber at time t_1 excites one set of reflectors. b) The same pulse at time t_2.

sketches that the region of the fiber which contributes to the backscattered signal at a given instant of time has a width $W/2$, where W is the spatial width of the pulse (A similar form for a continuous case can be derived [27]). Propagation of this region of width $W/2$ in the fiber is illustrated in Fig. 6.

We can also see that a particular point in the fiber will be excited for the whole duration of the pulse. This result has to be taken into account to consider temporal correlation effects, since the signals coming from different scatterers are independent from each other. This can be seen clearly from Fig. 6. The phase perturbation location is excited at time T and stops being excited at time $T + \Delta t$.

$$E_b(t, z = 0) = E_0 e^{i\omega t} \sum_{z_n = \frac{tv_g - W}{2}}^{\frac{tv_g}{2}} r_n e^{i(\varphi_n + \theta_p)} e^{-2\alpha z_n} e^{2i\beta z_n} \tag{2.1}$$

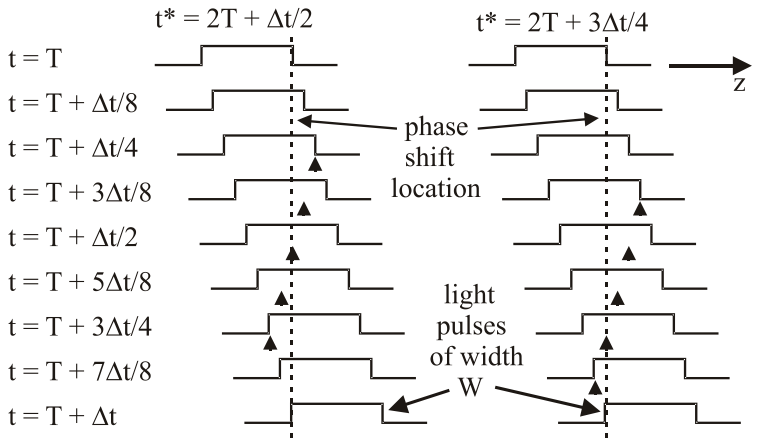

Fig. 5. Schematic illustration of the propagation of a light pulse in a fiber as it crosses a location at which a phase shift is applied. Each solid triangle indicates the location from which the backscattered light reaches the entrance end of the fiber at time $t*$.

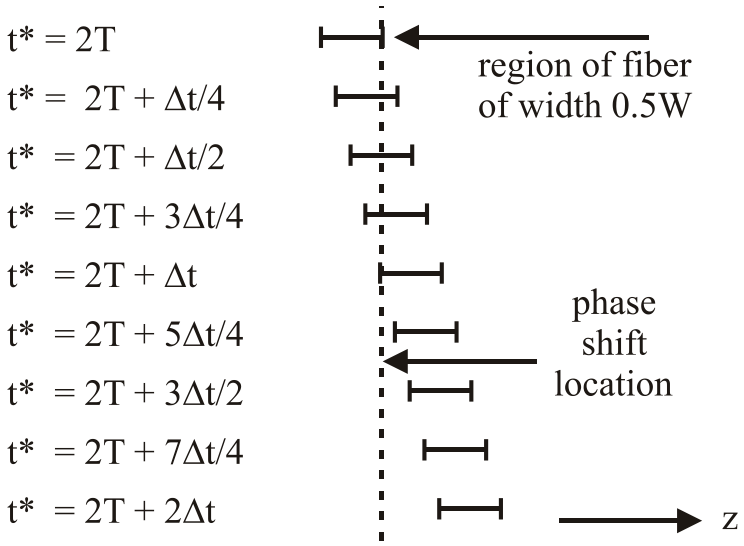

Fig. 6. Propagation of the region in the fiber of extent $0.5W$ for which backscattered light arrives at the entrance end of the fiber at time $t*$.

Where r_n is the reflectance of the n'th reflector, z_n is its position and α is the loss of the fiber. The parameter θ_p is the phase perturbation factor, only those scatterers that are after the phase perturbation will be affected. Or put in a mathematical form,

$$\theta_p = \begin{cases} 0, z_n < z_p \\ 2\varphi_p, z_n \geqslant z_p \end{cases} \tag{2.2}$$

Where z_p is the point where the perturbation occurs, and φ_p is the phase of the perturbation.

CHAPTER III

STATISTICS OF REFLECTIONS

A. Fabry-Perot Interferometer Model for the ϕ-OTDR

A ϕ-OTDR can be envisioned as a fiber Fabry-Perot interferometer with distributed reflectors of reflectance R_A and R_B, positioned on either side of a location at which a phase perturbation θ_{pert} is applied to the fiber, as illustrated in Fig. 7. In our model, the values of R_A and R_B at a particular instant in time result from coherent addition of electric field amplitudes of backward-propagating waves from a large number of randomly located reflectors in the fiber. When the leading edge of a light pulse reaches the phase shift location, the scatterers within the pulse initially contribute to R_A. As the pulse continues to propagate, the number of scatterers contributing to R_A diminishes while the number contributing to R_B grows. Finally, when the trailing edge of the pulse reaches the phase shift location, all of the scatterers within the pulse contribute to R_B.

As the fiber temperature or laser frequency changes with time, the phase relations between the contributions from the various reflectors also change, leading to changes in the values of R_A and R_B. Assuming that R_A and R_B are always $\ll 1$, which will be the case for the anticipated applications of the ϕ-OTDR, the reflected power R from such an interferometer can be expressed as

$$R = r_A^2 + r_B^2 + 2r_A r_B \cos(\phi_0 + 2\theta_{pert}) \tag{3.1}$$

where the amplitude refection coefficients r_A and r_B are related to the reflectances by

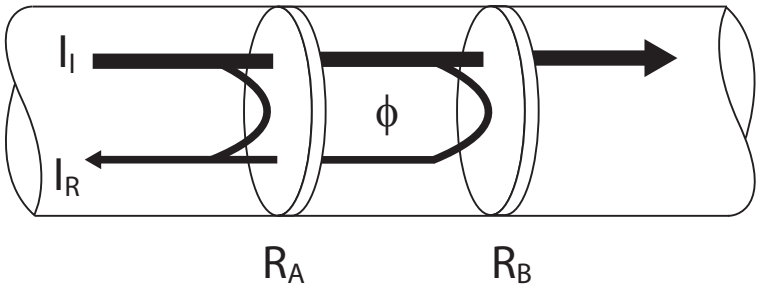

Fig. 7. Fabry-Perot model for a ϕ-OTDR. The incident light is reflected from two mirrors of reflectance R_A and R_B, with both reflectances $\ll 1$. The light reflected from the second mirror experiences a phase shitft of ϕ radians relative to the light reflected from the first mirror.

$$\begin{aligned} R_A &= \sqrt{r_A} \\ R_B &= \sqrt{r_B} \end{aligned} \tag{3.2}$$

and ϕ_0, the phase difference between the two reflected waves in the absence of an applied perturbation, is termed the phase bias. The value of ϕ_0 is determined by the coherent addition of the amplitudes of the waves from the individual reflectors, and is a random quantity with a uniform probability distribution over the range $0 < \phi_0 < 2\pi$ The factor of 2 multiplying θ_{pert} , which represents the phase perturbation induced by the intruder and defined in eq. (7.34), results from the fact that the return wave from the second reflector of reflectance R_B passes through the phase-shift region twice.

In the ϕ-OTDR, we are interested in the change in the trace resulting from the application of θ_{pert}. It follows from eq. (7.34) that, when the interferometer as a whole is considered, two types of fading can occur, which will be termed "reflectance fading" and "phase bias fading". Reflectance fading occurs when $r_A r_B$ is small, which occurs occasionally as the fiber temperature or laser frequency drift with time. Phase bias fading results when the value of ϕ_0 is such that the change in R given by eq.

(7.34) is small in response to an applied phase perturbation θ_{pert}. Reflectance fading can occur regardless of the value of ϕ_0.

B. Statistics of Reflections

In the linearly polarized (LP) mode approximation [26], a single mode fiber with its axis in the z-direction supports two orthogonally polarized waves with amplitudes $\mathbf{E}_x$ and $\mathbf{E}_y$ given by

$$\begin{aligned} \mathbf{E}_x(z,t) &= E_x(z)e^{i\omega t - i\beta_x z}\hat{x} \\ \mathbf{E}_y(z,t) &= E_y(z)e^{i\omega t - i\beta_y z}\hat{y} \end{aligned} \tag{3.3}$$

with $E_x(z)$ and $E_y(z)$ the field amplitudes, ω the radian frequency of the light, and β_x and β_y the mode propagation constants for the two polarization constants. In the ideal case of a cylindrically symmetric, isotropic fiber, the two propagation constants are equal. However, in actual cabled fibers, stresses and asymmetries lead to a slight birefringence; i.e., $\beta_x \neq \beta_y$.

Our model assumes that the amplitudes of the reflected waves for a particular (x or y) polarization from M reflectors, randomly located in the fiber, add coherently at the optical receiver to produce the detected optical power, according to

$$u = \sum_{m=1}^{M} u_m \tag{3.4}$$

where u is the resultant electric field amplitude of the reflected wave at the receiver, and u_m is the amplitude of the contribution from the m'th reflector. In this expression, relating to Eq.(2.1),

$$u_m = r_m e^{i(\varphi_m + \theta_p)} e^{2i\beta z_m} = A e^{i\phi_m} \tag{3.5}$$

where A is the amplitude of the contribution from each reflector, and $\{\phi_m\}$ are the phases of the reflected waves, $1 \leqslant m \leqslant M$. We can write

$$u_m = (u_m)_R + i(u_m)_I \tag{3.6}$$

where $(u_R)_m$ and $(u_I)_m$ are the real and imaginary parts of the field amplitude, given by

$$\begin{aligned} (u_m)_R &= A\cos\phi_m \\ (u_m)_I &= A\sin\phi_m \end{aligned} \tag{3.7}$$

As the temperature of the fiber changes, or the laser frequency drifts, the value of each ϕ_m will vary over the interval $0 < \phi_m < 2\pi$. The mean values of the quantities $(u_m)_R$ and $(u_m)_I$, denoted by $\langle(u_m)_R\rangle$ and $\langle(u_m)_I\rangle$, are given by

$$\langle(u_m)_R\rangle = \langle(u_m)_I\rangle = 0 \tag{3.8}$$

while

$$\langle(u_m)_R^2\rangle = \langle(u_m)_I^2\rangle = \frac{A^2}{2} \tag{3.9}$$

and

$$\langle|u_m|^2\rangle = A^2 \tag{3.10}$$

The addition of the M wave amplitudes is a random walk process, according to our model's assumptions, and it follows that, for $M \to \infty$,

$$\begin{aligned} \langle u_R \rangle &= \langle u_I \rangle = 0 \\ \langle u_R^2 \rangle &= \langle u_I^2 \rangle = \tfrac{MA^2}{2} \\ \langle |u|^2 \rangle &= MA^2 \end{aligned} \tag{3.11}$$

with u given by eq.(3.4).

Once again invoking the central limit theorem, the normalized probability distributions for u_R and u_I are Gaussian functions $P_G(u_R)$ and $P_G(u_I)$ and can be written

$$\begin{aligned} P_G(u_R) &= \sqrt{\tfrac{a}{\pi}} \exp(-a u_R^2) \\ P_G(u_I) &= \sqrt{\tfrac{a}{\pi}} \exp(-a u_I^2) \end{aligned} \tag{3.12}$$

where the constant a is given by

$$a = \frac{1}{MA^2}. \tag{3.13}$$

Alternative forms for these probability distributions are

$$\begin{aligned} P_G(u_R) &= \tfrac{1}{\sqrt{2\pi\sigma}} \exp(-u_R^2/2\sigma^2) \\ P_G(u_I) &= \tfrac{1}{\sqrt{2\pi\sigma}} \exp(-u_I^2/2\sigma^2), \end{aligned} \tag{3.14}$$

where the standard deviation σ is given by

$$\sigma = \frac{1}{\sqrt{2a}}. \tag{3.15}$$

From independence of the imaginary and the real part of u, we can write the probability distribution function [28]

$$P_G(u_R, u_I) = P_G(u_R) P_G(u_I) \tag{3.16}$$

Using the properties of Gaussian distribution, we can write

$$P_G(|u|) = P_G(u_R)P_G(u_I), \tag{3.17}$$

which, from eqs. (3.14) is given by

$$P_G(|u|) = \frac{a}{\pi}\exp(-a|u|^2) \tag{3.18}$$

In calculating average value of quantities of interest, it can be noted that the average value of a function $f(|u|)$, which is given by evaluating the integral

$$\langle f(|u|)\rangle = \int_{-\infty}^{\infty} du_R \int_{-\infty}^{\infty} du_I P_G(u_R)P_G(u_I)f(|u|) \tag{3.19}$$

can also be evaluated using the cylindrical coordinate representation of the integral, expressed as

$$\langle f(|u|)\rangle = 2\pi \int_{0}^{\infty} P_G(|u|)|u|f(|u|)du \tag{3.20}$$

It follows from eqs. (3.18) and (3.20) that

$$\langle |u|\rangle = 2a \int_{0}^{\infty} |u|^2 \exp(-a|u|^2)d|u|, \tag{3.21}$$

which, from integral tables is evaluated to be

$$\langle |u|\rangle = 0.5\sqrt{\frac{\pi}{a}} = \frac{0.886}{\sqrt{a}}. \tag{3.22}$$

Thus,

$$a = \frac{.25\pi}{\langle |u| \rangle^2}, \tag{3.23}$$

which makes it possible to express eq. (3.18) as

$$P_G(|u|) = \frac{.25}{\langle |u| \rangle^2} \exp(-.25\pi\mu^2), \tag{3.24}$$

with

$$\mu = \frac{|u|}{\langle |u| \rangle}. \tag{3.25}$$

C. Probability of Fading of the Signal

"Reflectance fading" will occur when the detected optical power from a region of the fiber falls to a very low value because the random phases $\{\phi_m\}$ for the individual reflectors are such that the resultant amplitude of the light wave at the optical receiver is close to zero. A measure of the extent to which this occurs is the probability that the magnitude of reflected amplitude $|u|$ is less than a particular value u_0, $P(|u| < u_0)$, given by

$$P(|u| < u_0) = 2\pi \int_0^{u_0} |u| P_G(|u|) d|u| \tag{3.26}$$

which, from eq.(3.24), is given by

$$P(|u| < u_0) = .5\pi \int_0^{\mu_0} \mu \exp(-.25\pi\mu^2) d\mu, \tag{3.27}$$

with

$$\mu_0 = \frac{u_0}{\langle |u| \rangle}. \tag{3.28}$$

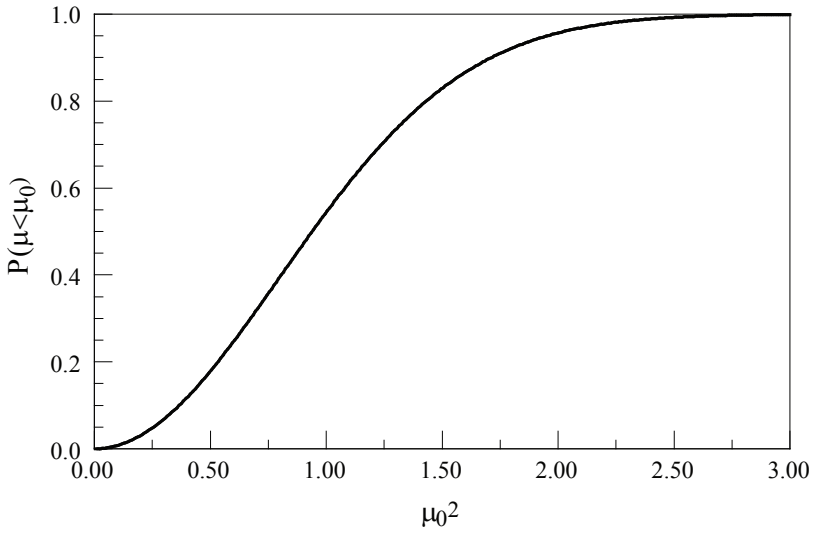

Fig. 8. Fading probability for a single reflector composed of many individual reflectors with random phase.

The integral in eq.(3.27) is evaluated to be

$$P(|u| < u_0) = 1 - \exp(-.25\pi\mu_0^2). \tag{3.29}$$

This expression is plotted in Fig. 8. Thus, in the limit of small μ_0,

$$P(|u| < u_0) \approx .25\pi\mu_0^2. \tag{3.30}$$

The preceding analysis applies to the statistics of the amplitude $|u|$ of the light wave reflected from a region of the fiber containing M reflectors. In the Fabry Perot model of the ϕ-OTDR introduced before, the quantity $|u|$ is analogous to one of the coefficients r_A and r_B, which represent the amplitudes of the light waves reflected from the two regions on either side of the location of the applied phase perturbation.

As mentioned in above, reflectance fading is related to the product $r_A r_B$. To treat this phenomenon, we introduce a new field amplitude variable v, which represents the sum of amplitudes reflected from a different region of the fiber than was used in computing $|u|$. The regions of the fiber used for computing u and v are adjacent to and on opposite sides of the location of the phase perturbation. By analogy with eq.(3.24),

$$P_G(|v|) = \frac{.25}{\langle |v| \rangle^2} \exp(-.25\pi\nu^2), \tag{3.31}$$

with

$$\nu = \frac{|v|}{\langle |v| \rangle} \tag{3.32}$$

We are interested in $P(\mu\nu < \gamma^2)$, where γ is a constant. The smaller the value of γ, the more severe the reflectance fading and the smaller the probability that such severe fading will occur. The region of fading in μ, ν space for two reflectors is illustrated in Fig. 9.

We need to integrate a two dimensional probability distribution, to find the expected value. We can see this more clearly using conditional probability notation and a discrete probability. In this case we have,

$$P(\mu\nu < \gamma^2) = \sum P(\mu\nu < \gamma^2 | \mu = x) P(\mu = x) \tag{3.33}$$

For the continuous case we have

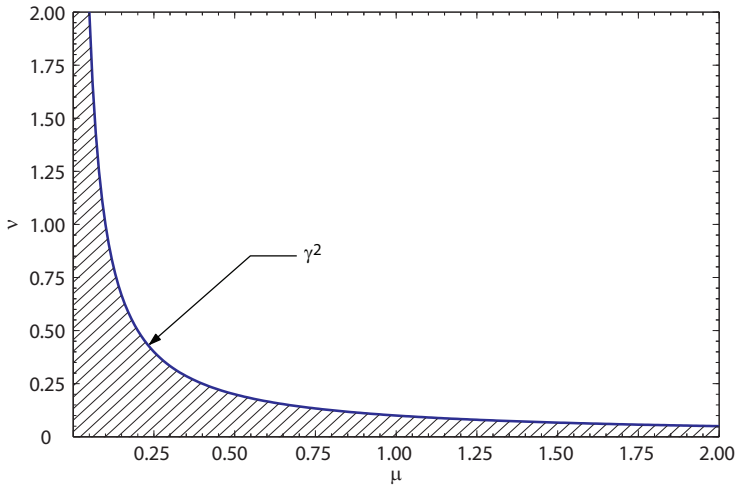

Fig. 9. The solid line represents the locus of μ and ν for which $\mu\nu = 0.1$ for fading in the case of two statistically independent reflectors. The probability has to be integrated over the shaded region.

$$\begin{aligned} P(\mu\nu \leqslant \gamma^2) &= .5\pi \int_0^\infty x \exp(-.25\pi x^2) P(\nu x \leqslant \gamma^2) dx \\ &= .5\pi \int_0^\infty x \exp(-.25\pi x^2) \int_0^{\gamma^2/x} .5\pi y \exp(-.25\pi y^2) dy dx \end{aligned} \tag{3.34}$$

We can rewrite this in a different way. To compute the probability of reflectance fading, we note that

$$P(\mu\nu < \gamma^2) = \langle P(\nu < \gamma^2/\mu) \rangle \tag{3.35}$$

with the expected value $\langle f(|u|) \rangle$ defined in eq.(3.19). If follows from eq. (3.31) that

$$P(\nu < \gamma^2/\mu) = 1 - \exp(-.25\pi\gamma^4/\mu^2). \tag{3.36}$$

Then, from eqs.(3.20), (3.24), and (3.36)

$$P(\mu\nu < \gamma^2) = .5\pi \int_0^\infty \mu[1 - \exp(-.25\pi\gamma^4/\mu^2)] \exp(-.25\pi\mu^2) d\mu. \tag{3.37}$$

Results for the dependence of P($\mu\nu < \gamma^2$) on γ^2 obtained by numerical evaluation of eq. (3.37) are plotted in Fig. 10. The first of these plots gives the result of this calculation with linear scales for both horizontal (abscissa) and vertical (ordinate) axes. The same data is replotted in Fig. 10b with a logarithmic scale for the vertical axis, as well as in Fig. 10c with a compressed horizontal axis.

The results given by eq.(3.37) and plotted in Fig. 10 give the probability for reflectance fading – the smaller the quantity γ^2, the more severe the fading. The analysis can be extended to include both reflectance and phase bias fading.

It follows from eq.(7.34) that the change in Fabry-Perot reflectance ΔR due to the application of a phase perturbation θ_{pert} is given by

$$\Delta R = 2r_A r_B[\cos(\theta_0 + 2\theta_{pert}) - \cos(\theta_0)], \tag{3.38}$$

It is possible to find the the probability distribution of the $cos(\Delta\phi_{ij})$. The process is illustrated in Fig. 11, where we graph the $cos(x)$ function in the interval $[-2\pi, 2\pi]$. Special care has to be taken, since $cos(\Delta\phi)$ is a multivalued function.

The Cumulative Distribution Function (CDF) of $cos(\Delta\phi)$ has the following form,

$$\begin{aligned} y &= \cos(x) \\ x &= \arccos(y) \\ F_y &= F_x(x_2) - F_x(x_1) + F_x(x_4) - F_x(x_3) \\ F_y &= F_x(-\arccos y) - F_x(\arccos y - 2\pi) \\ &\quad + F_x(2\pi - \arccos y) - F_x(\arccos y) \end{aligned} \tag{3.39}$$

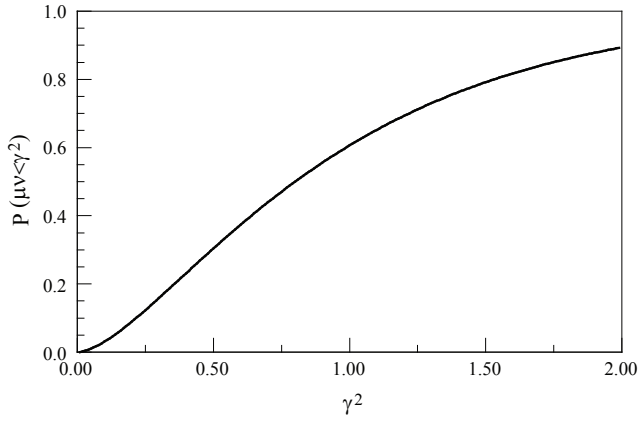

a)

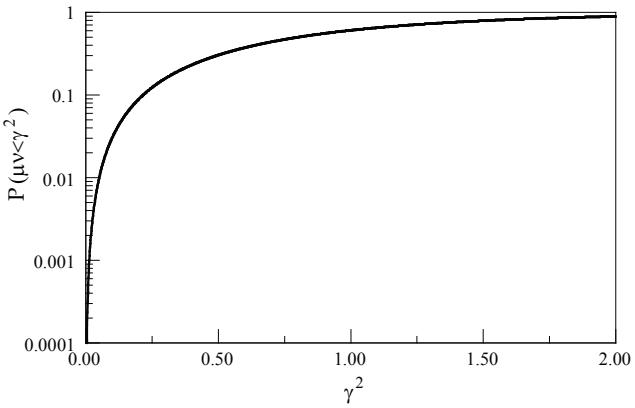

b)

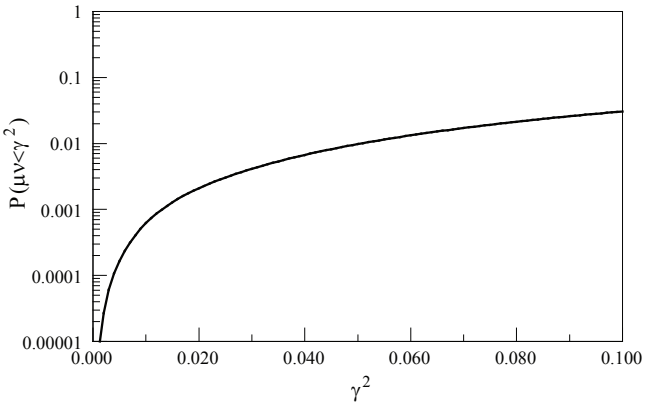

c)

Fig. 10. Dependence on γ^2 of the probability that $\mu\nu$ is less than γ^2: a) linear scale b) logarithmic scale for the vertizal axis, c) logarithmic scale for the vertical axis and compressed horizontal axis.

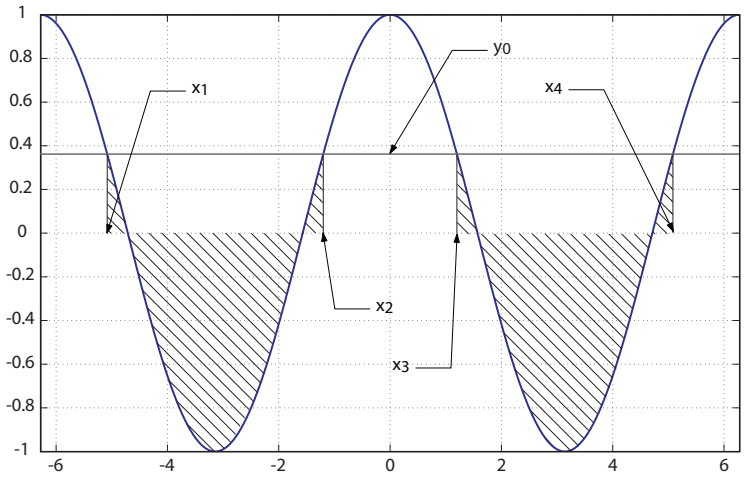

Fig. 11. Calculation of the PDF of $cos(\Delta\phi)$

where F_x is the CDF of a triangular distribution. The triangular distribution function of x comes from the fact that it's the difference between two uniformy distributed variates, in the $[-\pi, \pi]$ interval. The expression for F_x is given by

$$F_x(x) = \begin{cases} 0 & , x < -2\pi \\ \frac{(x+2\pi)^2}{8\pi^2} & , -2\pi \leqslant x \leqslant 0 \\ 1 - \frac{(2\pi - x)^2}{8\pi^2} & , 0 \leqslant x \leqslant 2\pi \\ 1 & , x > 2\pi \end{cases} \tag{3.40}$$

After some manipulation, we can show that,

$$F_y(y) = \begin{cases} 0\,,\ y < -1 \\ \left[1 - \frac{\arccos y}{\pi}\right]\,,\ -1 \leqslant y \leqslant 1 \\ 1\,,\ y > 1 \end{cases} \tag{3.41}$$

with y=cos($\Delta\phi$), which defines the CDF for the phase term in the Fabry-Perot model. The graph of eq.(3.41) is shown in Fig. 12. The probability distribution, can be found

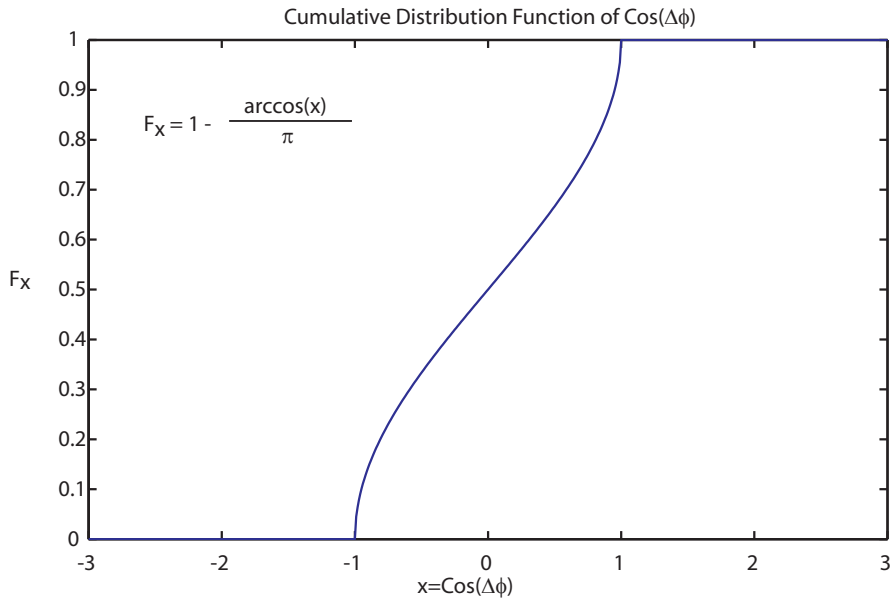

Fig. 12. CDF of $cos(\Delta\phi)$

by taking the derivative of the CDF, which, by using the double angle trigonometric identity, reduces to

$$\Delta R = 2r_A r_B[\cos\theta_0(\cos 2\theta_{pert} - 1) - \sin\theta_0 \sin 2\theta_{pert}], \tag{3.42}$$

The largest change in the magnitude of ΔR, when $\theta_{pert} = \pm 0.5\pi$ rad, is given by

$$|\Delta R| = 4r_A r_B|\cos\theta_0|. \tag{3.43}$$

In this case, severe phase bias fading occurs when $cos\theta_0 \approx 0$; i. e., if $\theta_0 \approx \pm\pi/2$. The value of θ_0 is determined by the random phases $\{\phi_n\}$ from the reflectors which contribute to the ϕ-OTDR trace. Thus, for calculating the fading probability it is assumed that θ_0 is a random quantity, $0 \leqslant \theta_0 < 2\pi$. Since we are concerned only with positive values of $cos\theta_0$, we can express the expectation value of a function $G(cos\theta_0)$ as

$$\langle G(\cos\theta_0)\rangle = \frac{2}{\pi}\int_{\theta_0=0}^{\pi/2} G(\cos\theta_0)d\theta_0. \tag{3.44}$$

We can then combine eqs. (3.37) and (3.44) to obtain

$$P(\mu\nu < 4\gamma^2|\cos\theta_0|) = \int_{\theta_0=0}^{\pi/2} d\theta_0 \int_0^{\infty} \mu[1-\exp(-\pi\gamma^4/64\mu^2\cos^2\theta_0)]\exp(-.25\pi\mu^2)d\mu. \tag{3.45}$$

Numerical evaluation of this expression is presented below, Fig.13, for comparison with Monte Carlo simulation results.

Simulation of the performance of the ϕ-OTDR starts with determining the random positions of the M reflectors within the fiber z_m, $m = 1,\ldots,M$, such that $0 < z_m < L$, with L the fiber length. Next, the corresponding phase shifts ϕ_m are determined from

$$\phi_m = \frac{4\pi n z_m}{\lambda}, \tag{3.46}$$

in the absence of a phase perturbation. Then, the values of u are calculated from eq.(3.4), and the backscattered power is proportional to $|u|^2$.The process is then repeated to take account of a phase perturbation by adding $2\phi_{pert}$ to only the values of the ϕ_m's from eq. (3.42) for which $z_m > z_{pert}$, where z_{pert} is the location of the perturbation. The new value of $|u|^2$ is then subtracted from the one calculated before the perturbation was applied to determine the effect of the perturbation. This difference is the signal of interest. The process of determining the random positions of reflectors and calculating the effect of ϕ_{pert} on $|u|^2$ is repeated many times to get

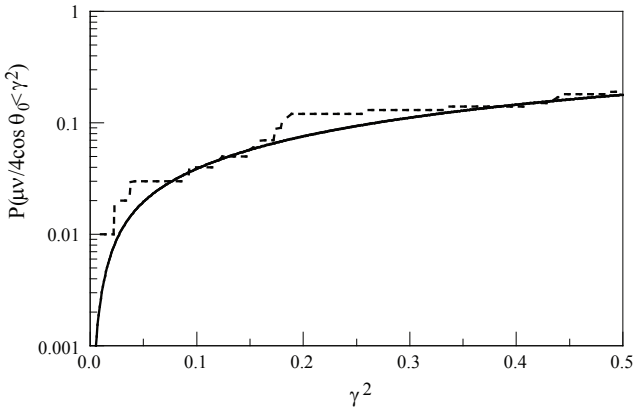

a)

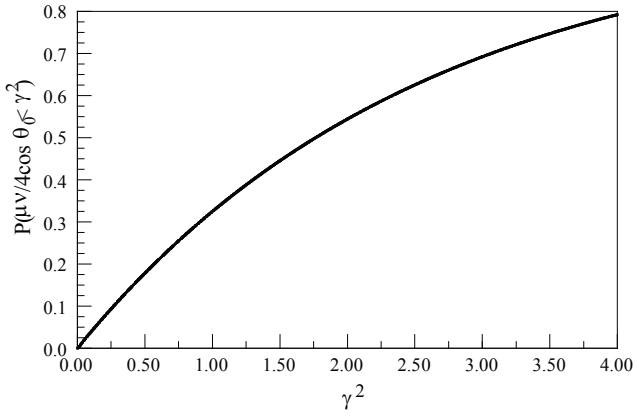

b)

Fig. 13. Comparison of a numerical calculation of fading probability from eq. 3.45 with the results of a Monte Carlo simulation: a) for 100 reflectors, b) for 1000 reflectors.

a statistical description of the signal from the ϕ-OTDR.

CHAPTER IV

CORRELATION AND STATISTICS OF THE DIFFERENCE BETWEEN PERTURBED AND UNPERTURBED SIGNALS

A. Probability Distribution of the Intensity

To analyze the phase fading, we will assume that the loss doesn't change considerably for the length of Δz. This approximation is good if the pulse is short enough. This is usually the case for a practical ϕ-OTDR system, where the length of the pulse is limited by the desired resolution, and the fiber presents low loss.

Taking an average of the positions of the scatterers z_m, inside the $\Delta z = W/2$ region, we can find,

$$\bar{z} = \langle z_m \rangle_{\Delta z}. \tag{4.1}$$

The approximation is a moving average of the loss over the spatial length of Δz. We notice that the time dependence is fully deterministic, and doesn't affect the statistics of the backscattered signal. If we fix the time, we have from eq.(2.1),

$$\begin{aligned} E_b(t = t_0, z = 0) &= E_0 e^{i\omega t_0} e^{-2\alpha \bar{z}} \sum_{z_n = \frac{tv_g - W_p}{2}}^{\frac{tv_g}{2}} r_n e^{i\varphi_n} e^{2i\beta z_n} \\ E_b &= E_0 e^{-2\alpha \bar{z}} E_{b_0} \\ E_{b_0} &= e^{i\omega t_0} \sum_{z_n = \frac{tv_g - W_p}{2}}^{\frac{tv_g}{2}} r_n e^{i\varphi_n} e^{2i\beta z_n} \end{aligned} \tag{4.2}$$

Rewriting eq. (4.2) in a more convenient form:

$$E_{b_0} = e^{i\omega t_0} \sum_{n=1}^{M} r_n e^{i\theta_n}. \tag{4.3}$$

The only random parameter is E_{b_0} and is the only one that contributes to fading. The variable of interest, that we can physically measure, is

$$\begin{aligned} I &= |e^{i\omega t_0}|^2 |E_{b_0}|^2 \\ &= |E_{b_0}|^2 \end{aligned} . \tag{4.4}$$

To analyze the statistical properties of the reflected signal, we proceed by analyzing the case when the number of reflectors M is equal to 3. This permits a detailed analysis and already shows the effects of coherence between signals. This result will be then generalized for an arbitrary M.

The expression for I_M in the case of three reflectors, $M = 3$, is,

$$\begin{aligned} |E|^2 &= |r_1 e^{i\phi_1} + r_2 e^{i\phi_2} + r_3 e^{i\phi_3}|^2 \\ &= |r_1 \cos(\phi_1) + r_2 \cos(\phi_2) + r_3 \cos(\phi_3) + \\ &\quad i(r_1 \sin(\phi_1) + r_2 \sin(\phi_2) + r_3 \sin(\phi_3))|^2 \end{aligned} \tag{4.5}$$

Expanding the absolute value and the square,

$$\begin{aligned} |E|^2 &= (r_1 \cos(\phi_1) + r_2 \cos(\phi_2) + r_3 \cos(\phi_3))^2 + \\ &\quad (r_1 \sin(\phi_1) + r_2 \sin(\phi_2) + r_3 \sin(\phi_3))^2 \\ &= r_1^2 + r_2^2 + r_3^2 + 2r_1 r_2 \cos\phi_1 \cos\phi_2 + 2r_1 r_3 \cos\phi_1 \cos\phi_3 + \\ &\quad 2r_2 r_3 \cos\phi_2 \cos\phi_3 + 2r_1 r_2 \sin\phi_1 \sin\phi_2 + 2r_1 r_3 \sin\phi_1 \sin\phi_3 + \\ &\quad 2r_2 r_3 \sin\phi_2 \sin\phi_3 \end{aligned} \tag{4.6}$$

By the use of trigonometric identities, we can see that,

$$\begin{aligned} |E|^2 = r_1^2 + r_2^2 + r_3^2 &+ 2r_1 r_2 \cos(\phi_1 - \phi_2) + 2r_1 r_3 \cos(\phi_1 - \phi_3) \\ &+ 2r_2 r_3 \cos(\phi_2 - \phi_3) \end{aligned} \tag{4.7}$$

We can generalize those expressions for an arbitrary M. It has to be noticed that

there won't be any terms involving the relations between three or more terms, since the sum is squared and no higher powers of the sum appear in the expression. For an arbitrary M, (A similar expression has been found in speckle [29]), we have,

$$I_M = \sum_{n=1}^{M} r_n^2 + 2 \sum_{i=1}^{M-1} \sum_{j=i+1}^{M} r_i r_j \cos(\phi_i - \phi_j). \tag{4.8}$$

Where $\Delta\phi_{ij} = \phi_i - \phi_j$ as the difference between the phases of two signals. This form is particularly useful when we want to find the correlation coefficient.

As it has been shown in Chapter III, the intensity for an arbitrary I_M will follow an exponential distribution. We can write this as,

$$P(I_M) = \frac{1}{M} \exp\left(\frac{-I_M}{M}\right) \tag{4.9}$$

for the Probability Distribution Function (PDF) of I_M. The corresponding expression for the CDF is,

$$F(I_M) = 1 - \exp\left(\frac{-I_M}{M}\right) \tag{4.10}$$

The Eqs. (4.9) and (4.10) match perfectly the distributions for $M > 8$, which can be shown by Monte Carlo simulations. The number of scatterers in practical systems is extremely large, $M \to \infty$, making the formulas particularly accurate.

B. Probability of the Intensity with a Phase Perturbation

If now we apply a phase perturbation, which is equal to twice the perturbation defined in Chpater III, $\theta_p = 2\phi_p$ (the 2 factor comes from the fact that the light has to cross that section two times), between the reflectors $q-1$ and q, we will have the next expression for the intensity,

$$I'_M = \sum_{i=1}^{M} r_i^2 + 2\sum_{i=1}^{q-2}\sum_{j=i+1}^{q-1} r_i r_j \cos(\phi_i - \phi_j) \\ +2\sum_{i=q}^{M-1}\sum_{j=i+1}^{M} r_i r_j \cos(\phi_i - \phi_j) + 2\sum_{i=1}^{q-1}\sum_{j=q}^{M} r_i r_j \cos(\phi_i - \phi_j - \theta_p) \tag{4.11}$$

Which is the contribution of the reflections from one side of the perturbation, then the other side. The last term is the contribution from the differences in phases of the reflectors on both sides of the perturbation.

The phase relations are illustrated in the Fig. 14. The term θ_p corresponds to the perturbation, and p is the fraction of scatterers before the perturbation to the total number of scatterers, p=4/8. In the Fig. 14a we can see, the $\Delta_{1,2} - \Delta_{1,4}$, which correspond to the terms before the perturbation, The Fig.18a only shows the terms between the first scatterer and those before the perturbation. In Fig. 14b we see the $\Delta_{5,6} - \Delta_{5,8}$, which are the terms after the perturbation, related to the fifth scatterer. Since both scatterers have the perturbation, when we take the difference between them, the perturbation cancels out. The last terms $\Delta_{1,5} - \Delta_{1,8}$ are the cross terms, shown in Fig. 14c. These are the only terms that present the perturbation, and as it will be shown later, they are the only ones that contribute to the detection of the signal.

In ϕ-OTDR the signal of interest is the difference between the intensities of two consecutive signals, one with a perturbation, the other one without it. We can use the eqs.(4.8) and (4.11), and take the difference between them,

$$I_M - I'_M = 2\sum_{i=1}^{q-1}\sum_{j=q}^{M} r_i r_j \cos(\phi_i - \phi_j) - 2\sum_{i=1}^{q-1}\sum_{j=q}^{M} r_i r_j \cos(\phi_i - \phi_j - \theta_p). \tag{4.12}$$

The expression can be simplified, eliminating those terms that are unchanged by

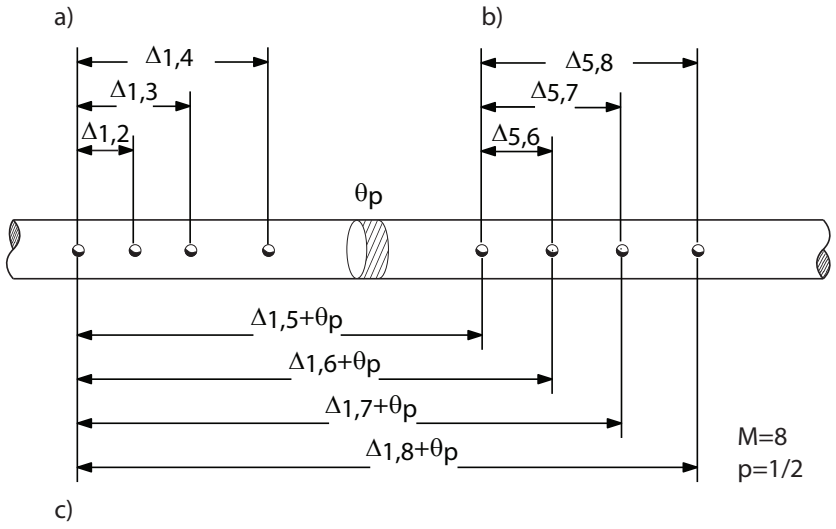

Fig. 14. Phase differences between scatterers. a) Phase differences before the perturbance. b) Phase differences before the perturbance. c) Cross terms from both sides of the perturbance.

the perturbation. The only terms left correspond to the cross terms on both sides of the perturbation,

$$I_M - I'_M \;=\; 2\sum_{i=1}^{q-1}\sum_{j=q}^{M} r_i r_j \left[\cos(\phi_i - \phi_j) - \cos(\phi_i - \phi_j - \theta_p)\right]. \tag{4.13}$$

We can present this term in a more convenient way

$$\begin{aligned} I_M - I'_M &= 2\sum_{i=1}^{q-1}\sum_{j=q}^{M} r_i r_j \left[\cos(\phi_i - \phi_j) - \cos(\phi_i - \phi_j)\cos\theta_p - \sin(\phi_i - \phi_j)\sin\theta_p\right] \\ &= 2\sum_{i=1}^{q-1}\sum_{j=q}^{M} r_i r_j \left[\cos(\phi_i - \phi_j)(1 - \cos\theta_p) - \sin(\phi_i - \phi_j)\sin\theta_p\right] \end{aligned} \tag{4.14}$$

For further analysis we will assume that all the reflectors have approximately the same value $r_i = r$. We can show that for the case M=2 the contributions to the intensity of light, from the variations of the reflectivity from their average value, only appear in a quadratic form. The average value for the reflectivity r, can be written

as,

$$r = \frac{r_1 + r_2}{2} \tag{4.15}$$

Then,

$$\begin{aligned} r_1 &= r - \delta r \\ r_2 &= r + \delta r \end{aligned} \tag{4.16}$$

From the equation of the intensity for the sum of two waves, eq.(4.8) we have

$$I = r_1^2 + r_2^2 + 2r_1 r_2 \cos \Delta\phi \tag{4.17}$$

By using eqs.(4.16), we have

$$\begin{aligned} r_1^2 &= (r^2 - 2r\delta r + \delta r^2) \\ r_2^2 &= (r^2 + 2r\delta r + \delta r^2) \\ r_1^2 + r_2^2 &= 2r^2 + 2\delta r^2 \\ 2r_1 r_2 &= 2(r^2 - r\delta r + r\delta r - \delta r^2) = 2(r^2 - \delta r^2) \end{aligned} \tag{4.18}$$

We can assume that $\delta r \ll r$. This assumption comes from the fact that most of the density fluctuations will be created under similar conditions of pressure and temperature during the pulling of the fiber. The quantities won't be exactly the same but they will be close to the average value, related to the loss of the fiber. Since δr is only present in a quadratic form, we can neglect it, resulting in the following equation:

$$\begin{aligned} I &= 2r^2 + 2r^2 \cos \Delta\phi \\ I &= 2r^2(1 + \cos \Delta\phi) \end{aligned} \tag{4.19}$$

We assume that such variations are negligible for any M, and that all the re-

flectivities are constant, which greatly simplifies the problem and permits further analysis.

It has been shown before that I_M follows an exponential distribution. In the perturbed case, the extra factor of phase doesn't modify its probability distribution, since the intensity will still be a sum of a large number of independent sines and cosines. This means that I'_M also follows an exponential distribution function, with the same average value M. Since only a portion of the factors is perturbed in I'_M, I_M and I'_M are correlated. This makes the signal of interest a random variable with the distribution function determined by the difference of two correlated random variables with exponential probability distribution function.

The correlation coefficient, that has to be determined, is defined as

$$\rho = \frac{\langle I_M I'_M \rangle - \langle I_M \rangle \langle I'_M \rangle}{\sqrt{Var(I_M) Var(I'_M)}} \tag{4.20}$$

Assuming that the scatterer density is constant, approximately $N = pM$ of the scatterers are localized between $[0, p]$ and are not affected by the phase shift. The remaining portion, $M - N = M(1-p)$ is localized between $[p, 1]$, and is perturbed. To be more accurate, the number of scatterers inside each section, $[0, p]$ and $[p, 1]$, would follow a binomial distribution. This won't be considered here, since it wouldn't modify the statistics of the signal considerably, but would complicate the model unnecessarily.

Using the equations above, we can find the correlation coefficient between I_M and I'_M. If we start with the case of $M = 4$, $q = 3$, assuming that p is the position of the perturbance in a normalized length $L = 1$, as above. Setting the parameter $p = 1/2$, which means that $N = 2$ reflectors are affected by the phase shift, and $M - N = 2$ are not, we have, from eqs.(4.8) and (4.11),

$$\begin{aligned}\langle I_M I'_M\rangle_{M=4} = \langle\{&4 + 2\cos\Delta\phi_{12} + 2\cos\Delta\phi_{13} + 2\cos\Delta\phi_{14} + 2\cos\Delta\phi_{23}\\ &+ 2\cos\Delta\phi_{24} + 2\cos\Delta\phi_{34}\}\\ &\times\{4 + 2\cos\Delta\phi_{12} + 2\cos(\Delta\phi_{13} - \theta_p) + 2\cos(\Delta\phi_{14} - \theta_p)\\ &+2\cos(\Delta\phi_{23} - \theta_p) + 2\cos(\Delta\phi_{24} - \theta_p) + 2\cos\Delta\phi_{34}\}\rangle.\end{aligned} \tag{4.21}$$

In order to evaluate the expected value, we use the following statistical properties of the terms in the sum:

$$\begin{aligned}&\langle a\rangle = a\\ &\langle\sin X\rangle = \langle\cos X\rangle = 0\\ &\langle\sin X\sin Y\rangle = \langle\sin X\rangle\langle\sin Y\rangle = 0\\ &\langle\cos X\cos Y\rangle = \langle\cos X\rangle\langle\cos Y\rangle = 0\\ &\langle\sin X\cos X\rangle = 0\\ &\langle a\sin^2 X\rangle = \langle a\cos^2 X\rangle = \tfrac{a}{2}\end{aligned} \tag{4.22}$$

Where X and Y are any of the original phase factors in the sum, and follow an uniform distribution in the $[-\pi, \pi]$ interval.

For example if we take one of the terms,

$$\begin{aligned}&\langle 2\cos\Delta\phi_{13} 2\cos(\Delta\phi_{13} - \theta_p)\rangle = 4\langle\cos(\phi_1 - \phi_3)\cos(\phi_1 - \phi_3 - \theta_p)\rangle\\ &= 4\langle\cos(\phi_1 - \phi_3)\cos(\phi_1 - \phi_3)\cos\theta_p + \cos(\phi_1 - \phi_3)\sin(\phi_1 - \phi_3)\sin\theta_p\rangle\\ &= 4\langle[\cos\phi_1\cos\phi_3 + \sin\phi_1\sin\phi_3][\cos\phi_1\cos\phi_3 + \sin\phi_1\sin\phi_3]\cos\theta_p\\ &\quad +[\cos\phi_1\cos\phi_3 + \sin\phi_1\sin\phi_3][\sin\phi_1\cos\phi_3 - \cos\phi_1\sin\phi_3]\sin\theta_p\rangle\\ &= 4\langle[\cos^2\phi_1\cos^2\phi_3 + 2\cos\phi_1\cos\phi_3\sin\phi_1\sin\phi_3 + \sin^2\phi_1\sin^2\phi_3]\cos\theta_p\\ &\quad +[\cos\phi_1\cos^2\phi_3\sin\phi_1 - \cos^2\phi_1\cos\phi_3\sin\phi_3 + \sin^2\phi_1\sin\phi_3\cos\phi_3\\ &\quad -\cos\phi_1\sin\phi_1\sin^2\phi_3]\sin\theta_p\rangle\end{aligned} \tag{4.23}$$

Using the linearity and independence properties, we have

$$\begin{aligned}\langle 2\cos\Delta\phi_{13} 2\cos(\Delta\phi_{13}-\theta_p)\rangle &= 4\cos\theta_p\left\{\langle\cos^2\phi_1\rangle\langle\cos^2\phi_3\rangle\right.\\ &\quad \left.+2\langle\cos\phi_1\sin\phi_1\rangle\langle\cos\phi_3\sin\phi_3\rangle+\langle\sin^2\phi_1\rangle\langle\sin^2\phi_3\rangle\right\}\\ &\quad +4\sin\theta_p\left\{\langle\cos\phi_1\sin\phi_1\rangle\langle\cos^2\phi_3\rangle\right.\\ &\quad -\langle\cos^2\phi_1\rangle\langle\cos\phi_3\sin\phi_3\rangle+\langle\sin^2\phi_1\rangle\langle\sin\phi_3\cos\phi_3\rangle\\ &\quad \left.-\langle\cos\phi_1\sin\phi_1\rangle\langle\sin^2\phi_3\rangle\right\}\\ &\quad =2\cos\theta_p\end{aligned} \tag{4.24}$$

Expanding the product, taking into account the fact that only those terms containing all of their terms in a quadratic form are different from zero, we have

$$\begin{aligned}\langle I_M I'_M\rangle_{M=4} &= \langle 16+4\cos^2\Delta\phi_{12}+4\cos\Delta\phi_{13}\cos(\Delta\phi_{13}-\theta_p)\\ &\quad +4\cos\Delta\phi_{14}\cos(\Delta\phi_{14}-\theta_p)+4\cos\Delta\phi_{23}\cos(\Delta\phi_{23}-\theta_p)\\ &\quad +4\cos\Delta\phi_{24}\cos(\Delta\phi_{24}-\theta_p)+4\cos^2\Delta\phi_{34}\rangle\end{aligned} \tag{4.25}$$

We notice that in addition to the constant related to the number of scatterers M^2, there are two terms without the perturbation factor. Those terms are the combination factors, on both sides of the perturbation, independent of each other. There are also four factors, which are the cross factors from both sides of the perturbation.

Using trigonometric identities and calculating the expected value term by term, we have

$$\langle I_M I'_M\rangle_{M=4} = 20+8\cos\theta_p \tag{4.26}$$

The expected value, from the characteristics of an exponential distributions func-

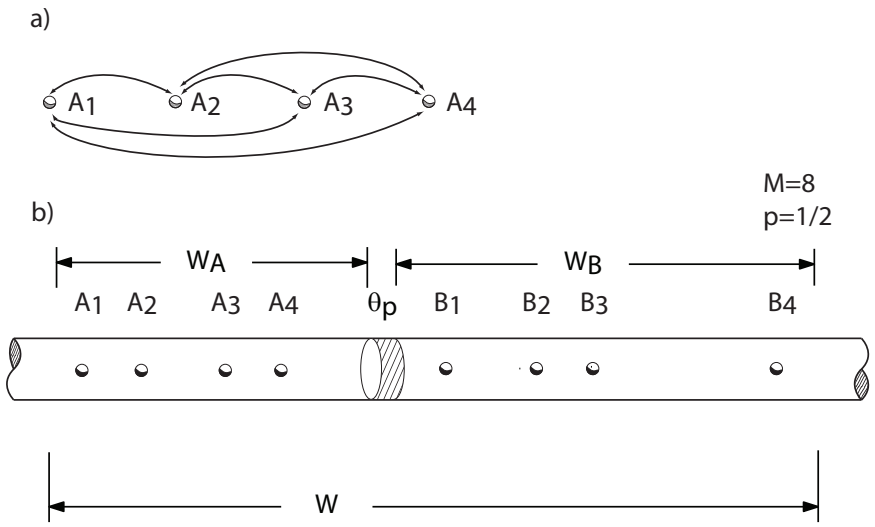

Fig. 15. Combinations of scatterers. a) Possible combinations for $M = 4$ b) Different groups of scatterers.

tion, is $\langle I_M \rangle = M$, and its variance is $Var(I_M) = M^2$, as has been shown before. In this case $M = M_1 = M_2$ since the number of scatterers didn't change, just a phase perturbation has been applied.

Continuing with the case M=4 and p=1/2, we can calculate the correlating coefficient, from eq.(4.20),

$$\rho_4 = \frac{20 + 8\cos\theta_p - M^2}{M^2} = \frac{1}{4} + \frac{1}{2}\cos\theta_p \tag{4.27}$$

We can generalize this result for an arbitrary M. First, we notice that the correlation coefficient is related to the number of reflectors on each side of the perturbation and the number of possible combinations between any two of them. The combinations calculations are illustrated in Fig. 15a, for the case of $M = 4$ scatterers. The total number of combinations in this figure is $N = 6$. For a general case we have,

$$N_T = \begin{pmatrix} M \\ 2 \end{pmatrix} = \frac{M!}{(M-2)!2!} = \sum_{i=1}^{M-1} i = \frac{M(M-1)}{2} \tag{4.28}$$

The next step is to find how many combinations are unperturbed. As shown on Fig. 15b the scatterers have to be divided into two groups, W_A and W_B. First consider the scatterers inside W_A by itself, then inside W_B by itself. If we add both numbers, we find the number of unperturbed terms. Under the assumption of a constant scatterer density, the number of scatterers inside both groups becomes: $W_A = pN$ and $W_B = (1-p)N$. The total number number of unperturbed terms becomes,

$$N_{NP} = \frac{pM(pM-1)}{2} + \frac{(1-p)M((1-p)M-1)}{2} \tag{4.29}$$

By subtracting the unperturbed terms from the total number of combinations inside W, we find the number of perturbed terms N_P. It would be possible to find directly this number, by considering all the possible cross combinations of two scatterers on both side of the perturbation.

$$N_P = N_T - N_{NP} = M^2 p(1-p) \tag{4.30}$$

This allows us to write the correlation coefficient

$$\rho = \frac{2}{M^2}\left(N_{NP} + N_P \cos\theta_P\right) \tag{4.31}$$

In the limit of $M \to \infty$ we can approximate the formula for ρ,

$$\begin{aligned} \rho_{M\to\infty} \approx \hat{\rho} &= 2p^2 - 2p + 1 + 2p(1-p)\cos\theta_p \\ \hat{\rho} &= \left[(1-p)^2 + p^2\right] + \left[2p(1-p)\right]\cos\theta_p \end{aligned} \tag{4.32}$$

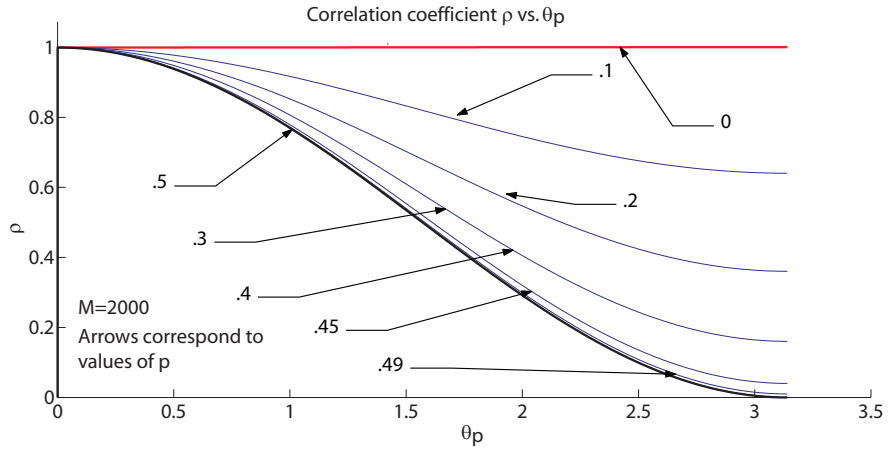

Fig. 16. Correlation coefficient.

The correlation coefficient ρ is a function of θ_p and p, we can make a plot of it versus those variables.

If the special case when the perturbation is exactly in the middle, $p = 1/2$, we can simplify the formula,

$$\hat{\rho}_{1/2} = \frac{1}{2} + \frac{1}{2}\cos\theta_p. \tag{4.33}$$

This case is of special importance, since it minimizes the correlation coefficient and maximizes the signal of interest. It will impose the limit of the performance of the system. A plot of the correlation factor is presented in Fig. 16.

The probability distribution function for the difference for two correlated random variables with exponential distribution function is [30],

$$P_\Delta(I) = \frac{\exp\left(\dfrac{I(M_1 - M_2) - |I|\sqrt{(M_1 - M_2)^2 + 4M_1M_2(1-\rho)}}{2M_1M_2(1-\rho)}\right)}{\sqrt{(M_1 - M_2)^2 + 4M_1M_2(1-\rho)}} \tag{4.34}$$

Where $\Delta = I_{M_1} - I_{M_2}$, I is the intensity of the difference, M_1 and M_2 are the

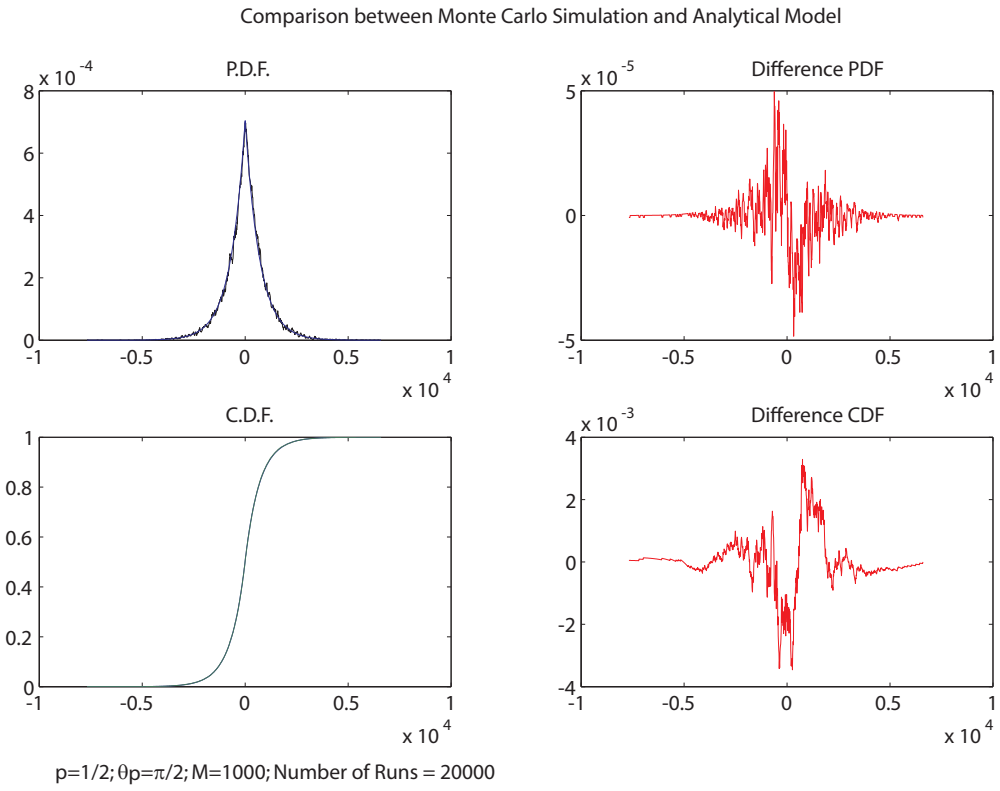

Fig. 17. Analytic model and Monte Carlo simulation comparison.

expected values of the two random variables, while ρ is their correlation coefficient.

In this case $M_1 = M_2 = M$, which reduces the formula (4.34) to,

$$P(I_M - I'_M) = \frac{1}{2M\sqrt{1-\rho}} \exp\left(\frac{-|I_\Delta|}{M\sqrt{1-\rho}}\right) \tag{4.35}$$

This gives the probability distribution of the signal of interest in ϕ-OTDR.

A comparison of this model with a Monte Carlo simulation is shown in Fig. 17. The model shows excellent agreement, which validates the formulas given above.

In the Appendix B the C++ code used for the Monte Carlo simulations is given, the results are plotted in Fig. 17. The program requires the use of *newran* library

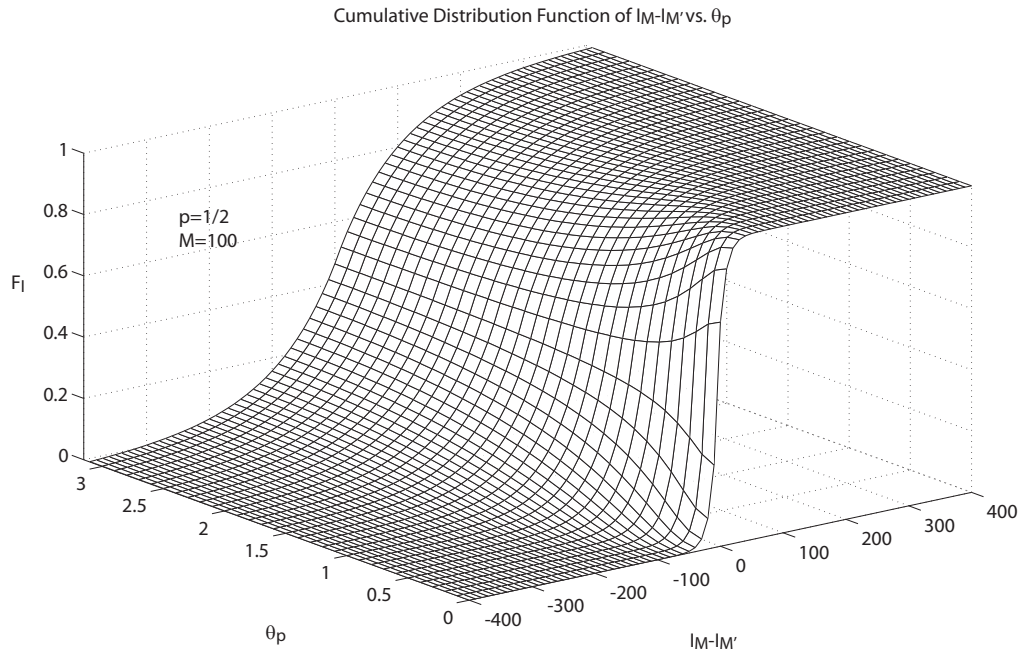

Fig. 18. CDF of the difference between the signals, for a fixed p.

[31], to generate random numbers. The main code is in *OTDRs.cpp*. This files makes makes use of a custom header file *custom.h*, to include the necessary libraries and defining suitable custom variables and classes.

The probability distribution function given by eq. (4.35) depends of two parameters. We can graph the cumulative distribution function of the signal of interest, versus both of them, as three dimensional graphs. Fig. 18 shows the graph of the CDF. for a fixed $p = 1/2$, the perturbation is in the middle, and varying all the other parameters.

We can see that when θ_p gets smaller, the probability of having a zero, which is equivalent of fading, grows. This can be seen since the slope of the curve gets steeper, making those values more probable. Fig. 19 shows the graph of the CDF for a fixed $\theta_p = \pi/2$, and changing p, the position of the perturbation. Similar conclusion can be

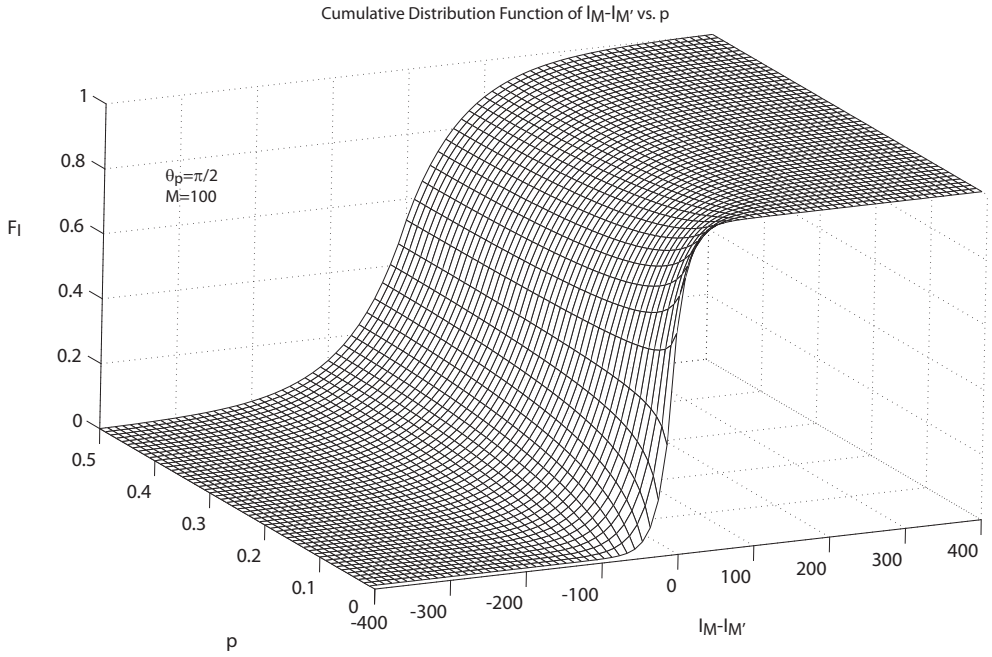

Fig. 19. CDF of the difference between the signals, for a fixed θ_p.

made from this graph, as from the previous one. If the perturbation is in the middle of the signal, the signal will be stronger.

We can see that the correlation time is equal to Δt, the duration of the pulse [16]. That is the time that a particular reflector is excited. This result is valid under the assumption that the scatterers are uncorrelated, which is the case in the present Rayleigh scattering model [3].

From the given expression for the probability P_I we can now calculate the probability of fading induced by the position and perturbation of the phase.

$$\begin{aligned} P(|I_\Delta| \leqslant I_{\Delta th}) &= \int_{-I_{\Delta th}}^{I_{\Delta th}} P_{I_\Delta}(I_\Delta) dI_\Delta = 2 \int_{0}^{I_{\Delta th}} P_{I_\Delta}(I_\Delta) dI_\Delta \\ &= 2 \int_{0}^{I_{\Delta th}} \frac{1}{2M\sqrt{1-\rho}} \exp\left(\frac{-|I_\Delta|}{M\sqrt{1-\rho}}\right) dI_\Delta \end{aligned} \tag{4.36}$$

Evaluating the integral

$$P_{Fad} = \frac{-M\sqrt{1-\rho}}{M\sqrt{1-\rho}} \exp\left(\frac{-|I_\Delta|}{M\sqrt{1-\rho}}\right)\Bigg|_{I_\Delta=0}^{I_{\Delta th}} = 1 - \exp\left(\frac{-|I_{\Delta th}|}{M\sqrt{1-\rho}}\right) \tag{4.37}$$

The expression above gives the probability that the absolute value of difference of signals is less than a certain threshold, I_{th}.

Extending the model by adding the loss term, that the intensity experiences as it propagates along the fiber, we have that

$$\Delta' = (I_{M_1} - I_{M_2})e^{-2\alpha\bar{z}}. \tag{4.38}$$

The exponential factor is deterministic and can be treated as a constant. The CDF of a random variable multiplied by a constant will be

$$F_y(y) = F_x(y/k) \tag{4.39}$$

We can see that the probability distribution function, using the fact that $e^{-2\alpha\bar{z}}$ is not a random quantity, has to be modified as follows

$$P(\Delta') = \frac{e^{2\alpha\bar{z}}}{2M\sqrt{1-\rho}} \exp\left(\frac{-|I_\Delta|e^{2\alpha\bar{z}}}{M\sqrt{1-\rho}}\right) \tag{4.40}$$

The probability of fading, defined in the same way as before, is

$$\begin{aligned} P(|I'_\Delta| \leqslant I_{\Delta th}) &= \int_{-I_{\Delta th}}^{I_{\Delta th}} P_{I'_\Delta}(I'_\Delta)dI'_\Delta = 2\int_{0}^{I_{\Delta th}} P_{I'_\Delta}(I'_\Delta)dI'_\Delta \\ &= 2\int_{0}^{I_{\Delta th}} \frac{e^{2\alpha\bar{z}}}{2M\sqrt{1-\rho}} \exp\left(\frac{-|I_\Delta|e^{2\alpha\bar{z}}}{M\sqrt{1-\rho}}\right)dI_\Delta \end{aligned}. \tag{4.41}$$

From which we can calculate,

$$P_{Fad} = \frac{-e^{2\alpha\bar{z}} M\sqrt{1-\rho}}{e^{2\alpha\bar{z}} M\sqrt{1-\rho}} \exp\left(\frac{-|I_\Delta| e^{2\alpha\bar{z}}}{M\sqrt{1-\rho}}\right)\Bigg|_{I_\Delta=0}^{I_{\Delta th}} = 1 - \exp\left(\frac{-|I_{\Delta th}| e^{2\alpha\bar{z}}}{M\sqrt{1-\rho}}\right) \quad (4.42)$$

For a constant threshold, the probability of fading of the signal, will be higher as the signal propagates in the fiber. Different threshold has to be used for the signal coming from different sections of the fiber. The signal from the far end needs a lower threshold than the signal from the end close to the source.

CHAPTER V

SHOT NOISE IN THE Φ-OTDR

The theory of the noise in photodetectors, widely applied in the analysis of bit error rates in optical communication systems, serves as the starting point for analyzing noise in the ϕOTDR. A simple photodetector circuit upon which the noise model is based is illustrated in Fig. 20.

It is assumed that the probability $P(N)$ for the number of electrons N delivered to a load impedance by a photodetector illuminated by a light source of constant power during a fixed sampling time τ is given by the Poisson distribution $P_P(N, \overline{N})$ [32]

$$P_P(N, \overline{N}) = \frac{e^{-\overline{N}} \left(\overline{N}\right)^N}{N!}, \tag{5.1}$$

where $N = 0, 1, \cdots$ and $\overline{N}$ is the average number of electrons per time interval (not

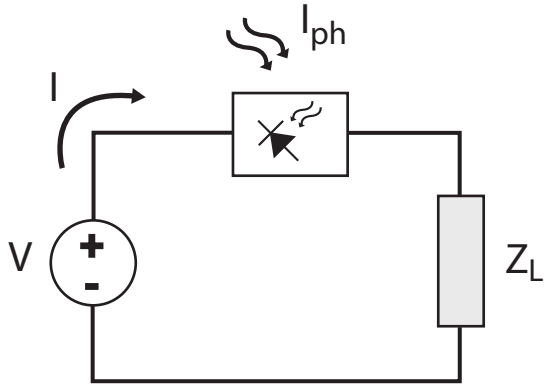

Fig. 20. Optical receiver, in which a photocurrent I, from a photodiode to which a DC bias volatge is applied, is induced by an input optical signal. The current is delivered to the receiver load impedance, Z_L.

necessarily an integer). It is easily shown that this expression satisfies the normalization condition

$$\sum_{N=0}^{\infty} P_P(N, \overline{N}) = 1. \tag{5.2}$$

for any $\overline{N}$.

If $\overline{N}$ is sufficiently large (let's say, $\overline{N} > 25$), as is usually the case in receivers for optical communication, the Poisson distribution in eq. (5.1) can be accurately approximated by the Gaussian distribution

$$P_G(N, \overline{N}) = \frac{1}{\sqrt{2\pi}\sigma} \exp\left(\frac{-(N-\overline{N})^2}{2\sigma^2}\right). \tag{5.3}$$

where σ is the standard deviation, given by

$$\sigma = \sqrt{\overline{N}}. \tag{5.4}$$

In a simple pulse code modulation optical communication system, in which a light pulse is emitted by the optical transmitter to transmit a "one" and no pulse is emitted to transmit a "zero", the average number of electrons from the photodetector will be designated $\bar{N}_1$ when a "one" is received and $\bar{N}_0$ when a "zero" is received. A threshold level N_{th} is set, such that

$$\overline{N}_0 < N_{th} < \overline{N}_1. \tag{5.5}$$

In the receiver circuitry, when N electrons are collected during a bit time interval τ, a decision is made that a "zero" was transmitted if $N < N_{th}$, and that a "one" was transmitted if $N > N_{th}$.

The bit error rate (BER) in such a system, assuming that the probability of error

is the same when a "zero" is transmitted as when a "one" is transmitted, is given by

$$BER = \int_{N_{th}}^{\infty} P_G(N, \overline{N}) dN, \tag{5.6}$$

with $P_G(N, \overline{N})$ given by eq.(5.3). Thus, the BER is the area under the tail of the Gaussian function. The "Q-function" $Q(\alpha)$, defined as

$$Q(\alpha) = \frac{1}{\sqrt{2\pi}} \int_{\alpha}^{\infty} \exp(-\zeta^2/2) d\zeta \tag{5.7}$$

is frequently used in characterizing bit error rates in communication systems. The graph of the function is shown in Fig.V. This function is normalized; i.e., $Q(-\infty) = 1$; and also has the property that $Q(0) = 0.5$. It follows from eqs. (5.3), (5.6), and (5.7) that

$$BER = Q\left(\frac{N_{th} - \overline{N}}{\sigma}\right). \tag{5.8}$$

It can be shown that for $\alpha > 4$, a good asymptotic approximation to Q(α) [33] is

$$Q(\alpha) \approx \frac{\exp(-\alpha^2/2)}{\sqrt{2\pi}\alpha}. \tag{5.9}$$

In the ϕ-OTDR, where detection of a phase shift is made by subtracting consecutive traces, the signal of interest ΔN is given by

$$\Delta N = N_+ - N_- \tag{5.10}$$

where N_- and N_+ are samples taken immediately before and after the phase shift was applied. If, in fact, no phase shift were applied, then ΔN represents the difference of two statistically independent samples from a distribution with mean $\overline{N}$. The resultant

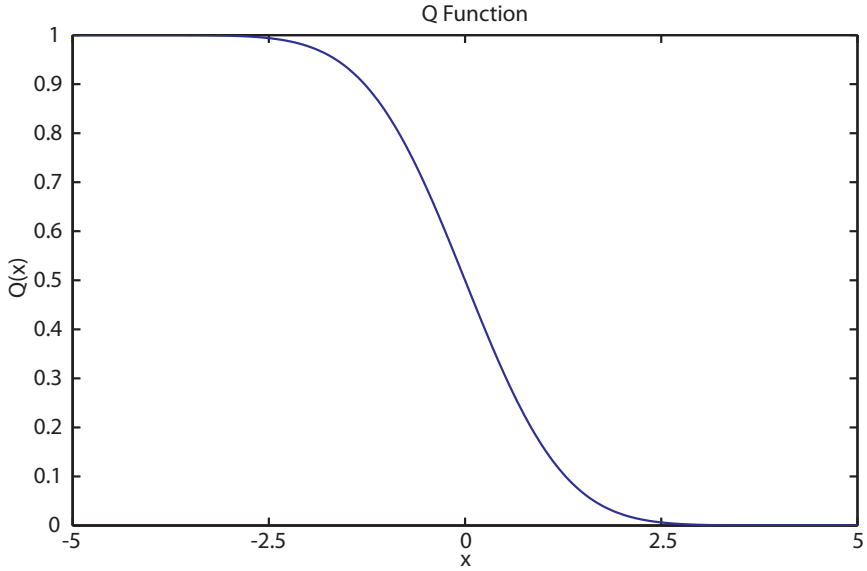

Fig. 21. Q function.

probability distribution for ΔN is then given by

$$P'_G(\Delta N) = \frac{1}{\sqrt{2\pi}\sigma'} \exp\left[\frac{-\Delta N^2}{2\sigma'^2}\right]. \tag{5.11}$$

where $\sigma\prime$ is the standard deviation for this Gaussian distribution, given by $\sigma' = \sqrt{2}\sigma$, or

$$\sigma' = \sqrt{2\overline{N}}. \tag{5.12}$$

A major difference between the ϕ-OTDR and most optical systems, including optical communication systems, is that the received optical power can vary randomly even in the absence of a signal, that is, if $\theta_{pert} \equiv 0$. This means that $\overline{N}$ can no longer be regarded as a constant, but rather as a statistically varying quantity. To determine the appropriate probability distribution for $\overline{N}$, we note from eq.(3.18) that the probability distribution for $|u|^2$ is a Gaussian function, with u the amplitude of

the optical signal at the receiver. This implies that the probability distribution for $\overline{N}$ can be written as the exponential function $P_E(\overline{N})$

$$P_E(\overline{N}) = C_1 \exp(-C_2\overline{N}), \tag{5.13}$$

with C_1 and C_2 constants. But normalization of $P_E(\overline{N})$ requires that $C_2 = C_1$. The expected value of $\overline{N}$, $\langle\bar{N}\rangle$, is evaluated from

$$\langle\bar{N}\rangle = \int_0^\infty \bar{N} P_E(\bar{N}) d\bar{N} \tag{5.14}$$

to be

$$\langle\bar{N}\rangle = \frac{1}{C_1} \tag{5.15}$$

so we can rewrite eq. (5.13) as

$$P_E(\overline{N}) = \frac{1}{\langle\overline{N}\rangle} \exp\left(-\frac{\bar{N}}{\langle\bar{N}\rangle}\right) \tag{5.16}$$

It follows from eq. (5.6) that

$$P(|\Delta N| > \Delta N_{th}) = 2\int_0^\infty P_E(\overline{N}) Q(\alpha) d\overline{N}, \tag{5.17}$$

with

$$\alpha = \frac{\Delta N_{th}}{\sqrt{2\overline{\overline{N}}}}, \tag{5.18}$$

which can be rewritten

$$\alpha = \frac{K}{\sqrt{X}}, \tag{5.19}$$

with

$$K = \frac{\Delta N_{th}}{\sqrt{2\langle \overline{N} \rangle}} \tag{5.20}$$

and

$$X = \frac{\overline{N}}{\langle \overline{N} \rangle}. \tag{5.21}$$

Then, using the approximate form for Q(α) from eq.(5.9), it follows that

$$Q(\alpha) = \frac{\sqrt{X}}{\sqrt{2\pi}K} \exp(-\frac{K^2}{2X}). \tag{5.22}$$

It then follows from eq.(5.17) that

$$P(|\Delta N| > \Delta N_{th}) = \frac{\sqrt{2}}{\sqrt{\pi}K} \int_0^\infty \sqrt{X} \exp(-X) \exp\left(-\frac{K^2}{2X}\right) dX, \tag{5.23}$$

This integral can be evaluated numerically to obtain the probability of the noise $|\Delta N|$ exceeding the threshold ΔN_{th}, for different values of K.

CHAPTER VI

PULSE POWER LIMITATIONS DUE TO BRILLOUIN SCATTERING

The optical signal level in a ϕ-OTDR, and hence the signal-to-noise ratio (SNR) and overall system performance improves as the optical power in a pulse of given duration increases. A phenomenon known as stimulated Brillouin scattering (SBS), which limits the maximum usable power in an optical fiber communication system, will have a similar effect on a ϕ-OTDR sensor system. SBS can affect the performance of the system by depleting the signal. It can also act as a noise source.

Brillouin scattering is an optical-acoustic interaction in which a photon of energy $h\nu$ interacts with the medium in which it propagates to emit or absorb a photon of energy $h\nu'$ and a phonon of energy E_{phon}. From the conservation of energy follows that

$$h\nu = h\nu' \pm E_{phon} \tag{6.1}$$

Although the description of the phenomenon requires a full quantum mechanical analysis, it has been found that for all practical purposes it can be described classically as the coupled interaction of the incident laser wave, an acoustic wave and the Brillouin scattered optical wave [34].

A. SBS in Single Mode Fibers

In our application, the duration of the pulse is much longer than the phonon lifetime, which is in the order of nanoseconds for optical fibers [35]. This allows us to treat the problem as a steady state SBS, and avoid transient analysis.

The steady state equations, after simplifying the equation and eliminating the

sounds wave dependence, governing SBS are [36]:

$$\begin{aligned} \frac{\partial I_L}{\partial z} &= -g_B I_L I_B - \alpha I_L \\ \frac{\partial I_B}{\partial z} &= -g_B I_B I_L + \alpha I_B \end{aligned} \tag{6.2}$$

where I_L and I_B are the signal and Brillouin intensities respectively, g_B is the Brillouin gain coefficient and α is the fiber attenuation coefficient. The coupled Eqs.(6.2) can be solved analytically if certain approximations are made, or integrated numerically [37].

B. Threshold of SBS in Single Mode Fibers

Classically, Brillouin scattering in optical fibers can be modeled as the amplification of thermally excited sound waves and propagates only in the backward direction. For sources with very narrow line width, Brillouin scattering is the main nonlinear effect and imposes limits to the transmitted power [38].

For light propagating in an optical fiber, SBS grows exponentially in the reverse direction when the optical power P exceeds a threshold P_{th}, given approximately by

$$P_{th} = \frac{21 A_{eff}}{g_B L_{eff}}. \tag{6.3}$$

where A_{eff} is the effective cross-sectional area of the fiber mode, g_B is the SBS coefficient, and L_{eff} is the maximum length of fiber over which the amplification occurs [39]. We have to keep the power below the threshold P_{th}, because if the power exceeds this threshold, the signal will be considerably depleted. It will be assumed here that the performance of the ϕ-OTDR is degraded when the SBS threshold is exceeded.

The value of L_{eff} is determined by the spatial width of the optical pulse W. Let

z_1 and z_2 be the location of the trailing and leading edge of the pulse, respectively, at a given time t_0, where

$$z_2 = z_1 + W \tag{6.4}$$

and

$$W = \frac{c\Delta T}{n_g}, \tag{6.5}$$

with c the free-space speed of light, n_g the group refractive index of the fiber mode, and ΔT the pulse duration. For $t > t_0$, light scattered from the front of the pulse at time t_0 will be located at z_2' given by

$$z_2' = z_2 - \frac{c(t - t_0)}{n_g}. \tag{6.6}$$

Amplification will cease at a time $\hat{t}$ when the scattered light at location z_2' passes the position z_1' of the forward-propagating pulse's trailing edge, given by

$$z_1' = z_1 + \frac{c(t - t_0)}{n_g} \tag{6.7}$$

Setting $z_1' = z_2'$ yields the result that

$$z_2 - z_1 = \frac{2c(\hat{t} - t_0)}{n_g} \tag{6.8}$$

It follows from eqs. (6.4) and (6.5) that

$$\hat{t} - t_0 = 0.5\Delta T \tag{6.9}$$

From the definitions of L_{eff} and z_1' that

$$L_{eff} = z_2 - z_1', \tag{6.10}$$

and from eqs. (6.4) and (6.7) that

$$L_{eff} = W - \frac{c(\hat{t} - t_0)}{n_g} \tag{6.11}$$

while from eqs. (6.5), (6.9), and (6.11) it follows that

$$L_{eff} = 0.5W \tag{6.12}$$

or, alternatively, from eq.(6.5),

$$L_{eff} = \frac{0.5c\Delta T}{n_g} \tag{6.13}$$

L_{eff} is the interaction length between the two signals.

C. Typical Single Mode Fiber

As an example, with $c = 3 \times 10^8$ m/s, $n_g = 1.46$ for silica fiber, it follows from eq. (6.13)that

$$L_{eff} = 1.027 \times 10^8 \Delta T \tag{6.14}$$

with L_{eff} in m and ΔT in s. For single mode fiber with an effective mode radius of 4 μm, the area is calculated to be

$$A_{eff} = 5.03 \times 10^{-11} m^2 \tag{6.15}$$

Using these values with $g_B = 5 \times 10^{-11}$ m/W [39], it follows from eq. (6.4) that

$$P_{th} = 2.06 \times 10^{-7}/\Delta T \tag{6.16}$$

Thus, the threshold optical power for SBS for a pulse width ΔT = 1 μs is

$$P_{th} = 206mW \tag{6.17}$$

The number of photons per optical pulse N_{phot} is given by

$$N_{phot} = \frac{P_{th}\Delta T}{h\nu} \tag{6.18}$$

with $h\nu$ the photon energy. It follows from eq.(6.16), with $h\nu = 1.28 \times 10^{-19}$ J at a wavelength of 1550 nm that

$$N_{phot} = 1.61 \times 10^{12} \tag{6.19}$$

This is the number of photons in a pulse for which the SBS threshold is predicted to occur. This value is independent of the pulse width. As indicated by eq.(6.16), the allowable laser power in the pulse is inversely proportional to the pulse width.

D. Spontaneous Brillouin Scattering (SpBS) as a Noise Source

Brillouin scattering below the P_{th} is usually called the spontaneous regime. The origin of SpBS from thermally excited acoustic phonons, subjected to random fluctuations,

make the scattered field noisy and unpredictable in nature.

Brillouin scattered field can be separated into two modes,

$$\begin{aligned} f_S &= f - \nu_B \\ f_A &= f + \nu_B \end{aligned} \tag{6.20}$$

where f_S and f_A are the frequencies of the Stokes and anti-Stokes components respectively, f is the frequency of the laser and ν_B is the Brillouin shift (typically close to 11 GHz for single mode silica fibers at $\lambda = 1.55$ μm). Only the Stokes component is amplified by SBS, this means that as long as the Stokes and anti-Stokes components have the same power, no Stimulated Brillouin Scattering is taking place [40].

In the spontaneous regime the Brillouin scattered power is linear with respect to the input power, similarly to the Rayleigh scattering. The ratio between both components (independent of the power of the source) depends on temperature and strain. The ratio is known as the Landau-Placzek ratio, and is defined as,

$$R_{LP} = \frac{I_R}{I_B} \tag{6.21}$$

where I_R and I_B are the Rayleigh and Brillouin intensities respectively. For single mode silica fibers, a typical value is $R_{LP} \approx 30$ at room temperature [40, 41].

Landau-Placzek ratio gives an estimate of I_B. To fully analyze the effects of the Brillouin phenomenon in the optical fiber, a more complete model has been developed [42]. The model considers the stimulated amplification of the noise by Brillouin scattering and its spectral characteristics. The extended model permits analyzing this effect as a noise source, taking into account the bandwidth and impedance of the receiver.

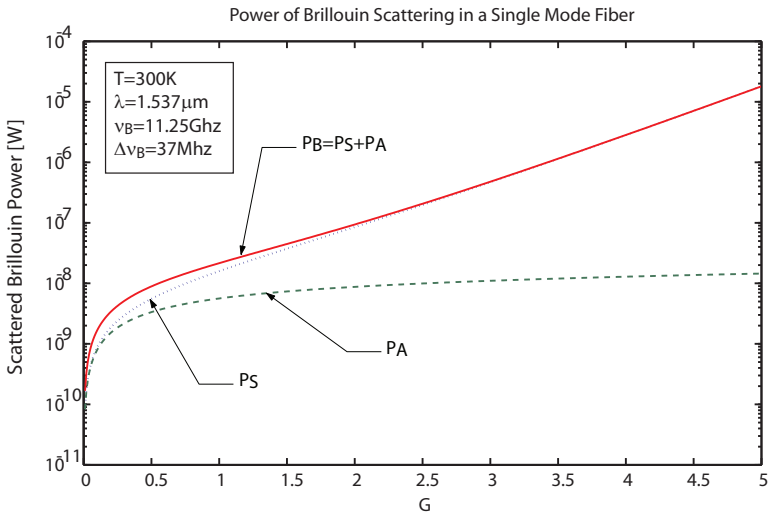

Fig. 22. Brillouin scattering intensity as function of G.

We start by defining a gain factor [43]:

$$G = (g_B P_P L_{eff})/(2A_{eff}) \tag{6.22}$$

The threshold defined in eq.(6.4) can be expressed, in terms of G, as

$$G_{th} \approx 10 \tag{6.23}$$

We can find backscattered Brillouin power as a function of G [43],

$$\begin{aligned} P_B(G) = [h\nu_S(\bar{n}+1))]\pi\Delta\nu_B G e^{G}[I_0(G) - I_1(G)] \\ + [h\nu_A\bar{n}]\,\pi\Delta\nu_B G e^{-G}[I_0(G) + I_1(G)] \end{aligned} \tag{6.24}$$

with $\Delta\nu_B$ being the Brillouin spectral bandwidth, ω_S and ω_A are the Stokes and anti-Stokes angular frequencies respectively, $\bar{n}$ is the phonon thermal equilibrium population, and I_0 and I_1 are the modified Bessel functions. The plot of P_B is shown in Fig. 22.

The phonon population in thermal equilibrium can be calculated from [42]

$$\bar{n} = \frac{1}{(e^{h\nu_B/kT} - 1)} \tag{6.25}$$

where $h = 6.626068 \times 10^{-34}$ J/s is the Planck's constant and $k = 1.3806505 \times 10^{-23}$ J/K is the Boltzmann's constant.

Since in practical systems the received power is limited by the properties of a photodetector, we have to write an expression of the power density of the detected electrical current. The optical power spectral density is,

$$\begin{aligned} \Phi_S(\omega) &= \hbar\omega_S(\bar{n}+1)\left(\exp\left(\frac{2(\pi\Delta\nu_B)^2 G}{(\pi\Delta\nu_B)^2 + (\omega-\omega_S)^2}\right) - 1\right) \\ \Phi_A(\omega) &= \hbar\omega_A\bar{n}\left(1 - \exp\left(\frac{-2(\pi\Delta\nu_B)^2 G}{(\pi\Delta\nu_B)^2 + (\omega-\omega_A)^2}\right)\right) \end{aligned} \tag{6.26}$$

where Φ_S and Φ_A are the optical power densities for Stokes and anti-Stokes scattering respectively. From the previous expression it's possible to find the spectral power density of the detected electrical current $\Psi_{S,A}$ (in $[A^2/Hz]$ and double sided) in terms of Φ_S or Φ_A as [43],

$$\begin{aligned} \Psi_{S,A} = {} & R^2 P_{S,A}^2 \delta\left(\tfrac{\omega}{2\pi}\right) + R^2 \left|H(\omega)\right|^2 \int_{-\infty}^{\infty} \Phi_{S,A}(\omega+\omega')\Phi_{S,A}(\omega')\tfrac{d\omega'}{2\pi} \\ & + eR\bar{g}FP_{S,A}\left|H(\omega)\right|^2 + \tfrac{1}{2}R^2 NEP^2 \left|H(\omega)\right|^2 \end{aligned} \tag{6.27}$$

where R is the photodetector's responsivity, $\bar{g}$ is its average gain, F is its excess noise factor, $H(\omega)$ is its spectral response, and NEP is its noise equivalent power. The first term in eq.(6.27) is the average current power detected; the second term represents the noise induced by the field statistics, the third term is the shot noise, and the fourth is the circuit noise contribution. The last three terms depend of the selected detection bandwidth.

E. Brillouin Scattering in Fiber Optic Sensor

In the optical sensor the SNR of the system increases with the laser power and its width. The width is limited by the spatial resolution of the system. It is not desirable to make the pulse too wide. SBS imposes the upper limit in the power of the pulse. It's possible to find the optimal power that would maximize the SNR as a function of G, defined by eq.(6.27).

The launched laser pulse will experiment loss as it propagates along the fiber, making the SNR dependent on the position in the fiber. This means that G decreases as the pulse propagates along the fiber. If we are interested in increasing the SNR of the signal at the end of the fiber, we can accept higher Brillouin noise from the first part of the fiber, in order to get a stronger signal from the far end.

CHAPTER VII

FRACTION OF INCIDENT OPTICAL POWER BACKSCATTERED INTO THE FIBER MODE

For a high-quality fused silica fiber, the optical loss in the near-infrared region of the spectrum is caused by Rayleigh scattering, resulting from microscopic inhomogeneities frozen into the fiber material when it cools from a semi-molten state during the drawing process. The present problem is concerned only with the part of the scattered field that is captured into a propagating mode and travels back in the fiber. This simplifies the problem since the exact form of the radiating components of the fields is not necessary.

A. Geometric Optics Approach

To calculate the fraction of the Rayleigh scattered light which is backscattered into the fiber mode, we consider a plane wave of wavelength λ incident in a medium of dielectric constant 1 on a dielectric sphere of dielectric constant ε and radius a, with $a \ll \lambda$. The solution to this classical problem in electromagnetic theory is represented in terms of the derivative of the Rayleigh scattering cross-section σ_{RS} per solid angle Ω as

$$\frac{d\sigma_{RS}}{d\Omega} = C(1 + \cos^2\theta) \tag{7.1}$$

with the constant C given by

$$C = \frac{2\pi^2 a^4(\varepsilon - 1)^2}{\lambda^2(\varepsilon + 2)^2}, \tag{7.2}$$

with θ the angle between the direction of propagation of the incident wave (+z direc-

tion) and the scattered wave [44]. The value of σ_{RS} is determined by evaluating the integral

$$\sigma_{RS} = \int \frac{d\sigma_{RS}}{d\Omega} d\Omega \tag{7.3}$$

over a solid angle of 4π radians, which can be expressed as

$$\sigma_{RS} = 2\pi C \int_0^{\pi} (1 + \cos^2\theta) \sin\theta d\theta. \tag{7.4}$$

Evaluation of this integral yields

$$\sigma_{RS} = \frac{16\pi C}{3}. \tag{7.5}$$

The direction of the incident wave corresponds to $\theta = 0$. Assuming that scattered light propagating at angles over the range $\pi - \theta_0 < \theta < \pi$ is captured by the fiber in the reverse direction, then the Rayleigh-backscattered cross section σ_{RBS} is given by

$$\sigma_{RBS} = 2\pi C \int_{\pi-\theta_0}^{\pi} (1 + \cos^2\theta) \sin\theta d\theta. \tag{7.6}$$

With the substitution $\theta' = \pi - \theta$, it follows that

$$\sigma_{RBS} = 2\pi C \int_0^{\theta_0} (1 + \cos^2\theta') \sin\theta' d\theta', \tag{7.7}$$

which is evaluated as

$$\sigma_{RBS} = 2\pi C \left[(1 - \cos\theta_0) + \frac{1 - \cos^3\theta_0}{3} \right], \tag{7.8}$$

For a single mode fiber the capture angle θ_0 can be assumed to be $\ll 1$, in which

case $\cos\theta_0 \approx 1 - \theta_0^2/2$ and eq. (7.8) reduces to

$$\sigma_{RBS} \approx 2\pi C\theta_0^2. \tag{7.9}$$

Thus, it follows from eqs. (7.5) and (7.9) that

$$\frac{\sigma_{RBS}}{\sigma_{RS}} = \frac{3\theta_0^2}{8}. \tag{7.10}$$

For a typical single mode fiber with $\theta_0 = 0.1$,

$$\sigma_{RBS} = .00375\sigma_{RS}. \tag{7.11}$$

B. Solution for the Step Index Fiber

The solution given above is the solution for a general case of any kind of fiber. In the case of a single mode step index fiber we can find a more exact solution. The solution follows that presented by Hartog et al. [45]. The coupling efficiency b is defined as

$$b(R_S) = \frac{1}{2}\frac{\left|\iint\limits_{2\pi} \psi_F\psi_S d\Omega\right|^2}{\iint\limits_{2\pi} |\psi_F|^2 d\Omega \iint\limits_{2\pi} |\psi_S|^2 d\Omega} \tag{7.12}$$

where R_S is the distance of the scatterer from the fiber axis, ψ_F and ψ_S are the far field distributions of the HE_{11} [46] mode and of the dipole, respectively, while $d\Omega$ is a solid angle differential.

The field distribution in this case is a Bessel function expression,

$$\psi_N(R) = \begin{cases} J_0(UR)/J_0(U), & R \leqslant 1 \\ K_0(WR)/K_0(W), & R \geqslant 1 \end{cases} \tag{7.13}$$

From this we have the expression for the captured fraction

$$B = 3\frac{W^4}{V^6}\frac{J_0^4(U)}{J_1^4(U)}\frac{(NA)^2}{n^2}\left[\int_0^1 R\frac{J_0^4(UR)}{J_0^4(U)}dR + \int_1^\infty R\frac{K_0^4(WR)}{K_0^4(W)}dR\right] \tag{7.14}$$

where R is the radial coordinate normalized to the core radius a, V is the normalized frequency, NA the numerical aperture, $W^2 = V^2 - U^2$, U is the eigenvalue, while n is the refractive index under the approximation $n_1 \simeq n_2 = n$.

The eigenvalue equation what has to be solved to find U is [47]

$$U\frac{J_1(U)}{J_0(U)} = W\frac{K_1(W)}{K_0(W)} \tag{7.15}$$

where J and K are Bessel functions. Eq.(7.15) is a transcendental equation and has to be solved numerically.

From the values given in the Appendix A, we can find that for a typical step-index single mode fiber used in $\phi - OTDR$ systems: $V \approx 2.2$, $U = 1.591$, $W = 1.519$, $NA = 0.144$, $n = 1.4682$. Which by direct evaluation of the eq.(7.14) gives $B = 2.15 \times 10^{-3}$.

This shows that the solution given by geometrical optics is accurate enough for practical purposes. The exact solution is of course impossible to obtain and impractical, since it would require the knowledge of the position and magnitude of each the scatterers inside the fiber and how they change with variations of temperature and pressure.

It is interesting to notice that an exact solution of a radiating dipole in a dielectric cylinder has been found [48, 49], but it can only be applied to single impurities, and is not valid for Rayleigh scattering, since it doesn't follow the λ^{-4} form [50].

C. Rate at Which Photons Are Backscattered into the Fiber Mode

Next, the photon backscattering rate $\frac{dN_{RBS}}{dt}$ (number of backscattered photons per unit time) will be calculated. The number of Rayleigh scattered photons dN_{RS} as the pulse propagates a distance dz in the fiber is given by

$$\frac{dN_{RS}}{dz} = \alpha_{RS} N_{pulse}, \tag{7.16}$$

with α_{RS} the Rayleigh scattering loss coefficient (units: length^{-1}) and N the number of forward-propagating photons in the pulse, given by

$$N_{pulse} = N_0 e^{-\alpha z}, \tag{7.17}$$

with N_0 the number of photons coupled into the fiber at $z = 0$, z the distance the pulse has propagated in the fiber, and α the length attenuation coefficient for the fiber, with $\alpha \geq \alpha_{RS}$. By convention the attenuation coefficient of a fiber is expressed in units of dB/km, and will be designated α'. The loss in dB, L_{dB}, is given by

$$L_{dB} = -10 \log_{10}(\frac{N_{pulse}}{N_0}), \tag{7.18}$$

and from eq. (7.17),

$$L_{dB} = 10\alpha z \log_{10} e \tag{7.19}$$

But

$$\alpha' = 0.001 \frac{dL_{dB}}{dz}, \tag{7.20}$$

where the factor 0.001 results because the length unit in α' is km^{-1}, while the length unit in α is m^{-1}. Since $log_{10}e = 0.4343$, it follows from eq.(7.19) and eq.(7.20) that

$$\alpha = 2.303 \times 10^{-4} \alpha' \tag{7.21}$$

But

$$\alpha'_{RBS} = \frac{\sigma_{RBS} \alpha'_{RS}}{\sigma_{RS}}, \tag{7.22}$$

and it follows from eqs.(7.11), (7.21) and (7.22) that

$$\alpha_{RBS} = 8.64 \times 10^{-7} \quad \alpha'_{RS}. \tag{7.23}$$

Using the value $\alpha'_{RS} = 0.20$ dB/km at a wavelength of $\lambda = 1550nm$, it follows that

$$\alpha_{RBS} = 1.73 \times 10^{-7}/m. \tag{7.24}$$

By analogy with eq. (7.16)

$$\frac{dN_{RBS}}{dz} = \alpha_{RBS} N_{pulse}, \tag{7.25}$$

The number of photons backscattered per unit time is given by

$$\frac{dN_{RBS}}{dt} = v_g \frac{dN_{RBS}}{dz}, \tag{7.26}$$

with v_g the group velocity of light in the fiber, given by

$$v_g = \frac{c}{n_g}, \tag{7.27}$$

where n_g is the group refractive index of the fiber mode. From eqs. (7.25),(7.26) and (7.27),

$$\frac{dN_{RBS}}{dt} = \frac{\alpha_{RBS} c N_{pulse}}{n_g}. \tag{7.28}$$

From eqs. (7.17), (7.24), (7.28) and , with $c = 3 \times 10^8$ m/s and $n_g = 1.46$ for a silica fiber, the number of Rayleigh-backscattered photons per second is given by

$$\frac{dN_{RBS}}{dt} = 35.5 N_0 e^{-\alpha z} \tag{7.29}$$

For example, if $N_0 = 10^{12}$, slightly below the threshold for SBS predicted by eq. (6.19), then

$$\frac{dN_{RBS}}{dt} = 3.55 \times 10^{13}. \tag{7.30}$$

at $z = 0$. The number of backscattered photons $N_{RBS}*$ which leaves the fiber at $z = 0$ is reduced from the value given in eq. (7.29) by the attenuation in the fiber, and is given by

$$\frac{dN_{RBS}*}{dt} = 35.5 N_0 e^{-2\alpha z} \tag{7.31}$$

The optical power $P*$ in the backscattered wave at $z = 0$ is expressed as

$$P* = h\nu \frac{dN_{RBS}*}{dt}, \tag{7.32}$$

so that

$$P* = 35.5 h\nu N_0 e^{-2\alpha z} \tag{7.33}$$

For example, at the entrance end of the fiber ($z = 0$), with $h\nu = 1.28 \times 10^{-19}$ J at a wavelength of 1550 nm, and $N_0 = 10^{12}$, the backscattered power is calculated to be

$$P* = 4.54\mu W \tag{7.34}$$

If the fiber loss is entirely due to Rayleigh backscattering, such that $\alpha' = \alpha'_{RBS} = 0.2dB/km$, then the round trip attenuation $e^{-2\alpha z}$ is 10 dB for each 25 km of fiber length. In our example, the backscattered power from a distance $z = 25$ km is 10% of the value in eq. (7.34), or

$$P* = 454nW \tag{7.35}$$

CHAPTER VIII

CONCLUSIONS

This dissertation focuses on the statistics of the signal in a ϕ-OTDR system, from the classical point of view. As has been shown the number of photons is large enough, so we can neglect quantum effects of the interactions between photons and matter. The equations for the statistical analysis of the backscattered signal have been derived. The noise power and bit error rate probabilities have been calculated, giving theoretical limits of performance for the system.

The operation of the system relies on the coherence of the laser source. Without coherent interference it wouldn't be possible to detect a phase perturbation caused by an intruder stepping on the fiber. The interference phenomena have the drawback of being random in nature, which leads to fluctuations and possibly a complete fading of the signal. In this case the fading is closely related to the fact that the signal originate from a random sum of a large number of waves.

Two different models have been developed. The first model, called the Fabry-Perot model, gives the probability that the full ϕ-OTDR signal fades, depending on the spatial position of the scatterers inside the fiber. This model considers the signal from both sides of the perturbation and predicts the fading of the signal taking into account the relative phases between them. The derivation of the statistics of the signal has been used to model the quantum noise in the photodetector and to give a statistical description of its behavior.

An alternative model has also been developed. This model gives the probability of the difference between two consecutive signals. In the case of ϕ-OTDR, this is the signal of interest. The model allows us to calculate the probability of the signal being below some chosen threshold. We can also see that noise and fiber loss play a

fundamental role, even in fading considerations. From this model we can calculate the probability that the signal fades depending of the phase and position of the perturbation. The correlation between two consecutive signals, one perturbed and one unperturbed had to be derived, and integrated into the derivations. The inclusion of loss into the model, shows that the probability of fading for a fixed threshold from the back of the fiber, is greater that if the intruder steps on the closer end of the fiber.

Another important aspect of the system has been calculated. The fraction of the Rayleigh backscattered signal that is guided back into the fiber. This allows a quantitative estimation of the order of powers expected in a real system. The model uses a general geometrical optics approach, which permits its extension to different kinds of fibers. Its accuracy has been validated with a full wave solution for a single mode step index fiber.

Brillouin scattering presents the limit for the power launched into the fiber, above which there will be serious depletion of the source as well as noise in form of Stokes and anti-Stokes waves. Brillouin scattering can represent a source of noise as well, through the stimulation of thermal waves. The model presented here permits the calculation of the contribution of this noise considering the bandwidth of the photodetector.

The present analysis covers most of the aspects of noise in the ϕ-OTDR. It also explains the coherent phenomena, under a monochromatic source assumption, governing the operation of the systems and its limitations. This permits the optimization of the system from a theoretical point of view, and gives a good insight of the mechanism behind the whole system.

The fading phenomena could be reduced by the addition of a second source with a different frequency. The probability of fading of both of the signals at the same time is much smaller than of one signal. In this case further analysis of four wave mixing and noise effects would have to be analyzed. The cost effects of having a

second source would have to be considered.

The next step of this work is to compare the models with a real implementation. This would allow the development of a more accurate model. The model can be expanded for physical variables not considered here, for example the effect of temperature, sound waves and vibrations in the system. A detailed analysis of large set of data from the sensor, with the simultaneous monitoring of other parameters would permit improving the overall performance of the system. The analysis would require a statistical point of view, analogous to the methods used here and the corresponding simplifications. The loss of the fiber depends of the drawing process. Recent works have focused on reducing the Rayleigh scattering losses in the fiber by modifying the temperature at which the fiber is created [51]. Incorporation in the model of thermodynamic effects would permit a better estimation of the properties in the fiber. The estimation of the size, number and intensity of the scatter centers would allow a closer analysis of the coherent interaction between them.

REFERENCES

[1] M. K. Barnoski and S. M. Jensen, "Fiber waveguides: a novel technique for investigating attenuation characteristics," *Applied Optics*, vol. 15, no. 9, pp. 2112–2115, Sep. 1976.

[2] D. Philen, I. White, J. Kuhl, and S. Mettler, "Single-mode fiber OTDR: experiment and theory," *IEEE Journal of Quantum Electronics*, vol. QE-18, no. 10, pp. 1499–1508, Oct. 1982.

[3] D. Marcuse, *Principles of Optical Fiber Measurements*. New York: Academic Press.

[4] I. Fabelinskii, *Molecular Scattering of Light*. New York: Plenum Press, 1968.

[5] J. Schroeder, "Light scattering of glass," in *Glass I: Interaction With Electromagnetic Radiation*, ser. Treatise on Materials Science and Technology Vol.12, M. Tomozawa and R. H. Doremus, Eds. New York: Academic Press, 1977, pp. 157–222.

[6] M. E. Lines, "Scattering losses in optic fiber materials. I. A new parametrization," *Journal of Applied Physics*, vol. 55, no. 11, pp. 4052–4057, Jun. 1984.

[7] T. R. Parker, M. Farhadiroushan, V. A. Handerek, and A. J. Rogers, "A fully distributed simultaneous strain and temperature sensor using spontaneous Brillouin backscatter," *IEEE Photonics Technology Letters*, vol. 9, no. 7, pp. 979–981, Jun. 1997.

[8] S. Kim, J. Lee, and I. Kwon, "Structural monitoring of a bending beam using Brillouin distributed optical fiber sensors," *Smart Materials and Structures*, vol. 11, pp. 396–403, May 2002.

[9] H. Taylor, "Fiber optic sensors based upon the Fabry-Perot interferometer," in *Fiber Optic Sensors*, F. Yu and S. Yin, Eds. New York: Marcel Dekker, 2002, pp. 41–74.

[10] A. Kung, J. Budin, L. Thevenaz, and P. A. Robert, "Rayleigh fiber optics gyroscope," *IEEE Photonics Technology Letters*, vol. 9, no. 7, pp. 973–975, Jul. 1997.

[11] C. Preininger, I. Klimant, and O. S. Wolfbeis, "Optical fiber sensor for biological oxygen demand," *Analytical Chemistry*, vol. 66, pp. 1841–1846, Jun. 1994.

[12] T. Bae, R. Atkins, H. Taylor, and W. Gibler, "Interferometric fiber-optic sensor embedded in a spark plug for in-cylinder pressure measurement in engines," *Applied Optics*, vol. 42, no. 6, pp. 1003–1007, Feb. 2003.

[13] Y. Xie and Y. Fang, "A general statistical channel model for mobile satellite systems," *IEEE Transactions on Vehicular Technology*, vol. 49, no. 3, pp. 744–752, May 2000.

[14] H. Izumita, S. Furukawa, Y. Koyamada, and I. Sankawa, "Fading noise reduction in coherent OTDR," *IEEE Photonics Technology Letters*, vol. 4, no. 2, pp. 201–203, Feb. 1992.

[15] S. K. Sheem, T. G. Giallorenzi, and K. Koo, "Optical techniques to solve the signal fading problem in fiber interferometers," *Applied Optics*, vol. 21, no. 4, pp. 689–693, Feb. 1982.

[16] P. Healey, "Fading in heterodyne OTDR," *Electronics Letters*, vol. 20, no. 1, pp. 30–32, Jan. 1984.

[17] ——, "Fading rates in coherent OTDR," *Electronics Letters*, vol. 20, no. 11, pp. 443–444, May 1984.

[18] K. Choi and H. Taylor, "Spectrally stable Er-fiber laser for application in phase-sensitive optical time-domain reflectometry," *IEEE Photonics Technology Letters*, vol. 15, no. 3, pp. 386–388, Mar. 2003.

[19] T. H. Wood, R. A. Linke, B. L. Kasper, and E. C. Carr, "Observation of coherent Rayleigh noise in single-source bidirectional optical fiber systems," *Journal of Lightwave Technology*, vol. 6, no. 2, pp. 346–351, Feb. 1988.

[20] G. P. Lees, P. C. Wait, M. J. Cole, and T. P. Newson, "Advances in optical fiber distributed temperature sensing using the Landau-Placzek ratio," *IEEE Photonics Technology Letters*, vol. 10, no. 1, pp. 126–128, Jan. 1998.

[21] X. Pan, P. F. Barker, A. Meschanov, J. H. Grinstead, M. N. Schneider, and R. B. Miles, "Temperature measurements by coherent Rayleigh scattering," *Optics Letters*, vol. 27, no. 3, pp. 161–163, Feb. 2002.

[22] L. Mandel and E. Wolf, *Optical Coherence and Quantum Optics*. Cambridge: Cambridge University Press, 1995.

[23] J. Juarez and H. Taylor, "Distributed fiber optic intrusion sensor system for monitoring long perimeters," in *Proc. SPIE*, vol. 5778, Orlando, FL, 2005.

[24] J. Juarez, E. Maier, K. Choi, and H. Taylor, "Distributed fiber-optic intrusion sensor system," *Journal of Lightwave Technology*, vol. 23, no. 6, pp. 2081–2087, Jun. 2005.

[25] L. Goldberg, H. F. Taylor, and J. F. Weller, "Feedback effects in a laser diode due to Rayleigh backscattering from an optical fibre," *Electronics Letters*, vol. 18,

no. 9, pp. 353–354, Apr. 1982.

[26] D. Gloge, "Weakly guiding fibers," *Applied Optics*, vol. 10, no. 10, pp. 2252–2258, Oct. 1971.

[27] R. M. Howard, "Statistics of coherently detected backscatter and range performance of coherent OTDRs," *Optical and Quantum Electronics*, vol. 19, pp. 145–168, May 1987.

[28] A. Papoulis, *Probability, Random Variables and Stochastic Processes*. New York: McGrawHill, 1965.

[29] D. Zimnyakov and M. Vilensky, "Blink speckle spectroscopy of scattering media," *Optics Letters*, vol. 31, no. 4, pp. 429–431, Feb. 2006.

[30] H. Holm and M.-S. Alouini, "Sum and difference of two squared correlated Nakagami variates in connection with the McKay distribution," *IEEE Transactions on Communications*, vol. 52, no. 8, pp. 1367–1376, Aug. 2004.

[31] R. B. Davies, "Newran02B - A random number generator library," [Online], 2002, Avialable: http://www.robertnz.net/nr02doc.htm.

[32] P. Russer, "Introduction to optical communications," in *Optical Fibre Communications*, M. Howes and D. Morgan, Eds. New York: John Wiley & Sons, 1980, pp. 1–26.

[33] W. Gautschi, "Error function and fresnel integrals," in *Handbook of Mathematical Functions*, M. Abramovitz and I. Stegun, Eds. New York: Dover, 1965, pp. 295–329.

[34] D. Cotter, "Stimulated Brillouin scattering in monomode optical fiber," *Journal of Optical Communications*, vol. 4, no. 1, pp. 10–19, Jan. 1983.

[35] J. Smith, A. Brown, M. DeMerchant, and X. Bao, "Pulse width dependance of the Brillouin loss spectrum," *Optics Communications*, vol. 168, pp. 393–398, Sep. 1999.

[36] S. L. Floch and P. Cambon, "Theoretical evaluation of the Brillouin threshold and the steady-state Brillouin equations in standard single-mode optical fibers," *Journal of the Optical Society of America A*, vol. 20, no. 6, pp. 1132–1137, Jun. 2003.

[37] L. Chen and X. Bao, "Analytical and numerical solutions for steady state stimulated Brillouin scattering in a single-mode fiber," *Optics Communications*, vol. 152, pp. 65–70, Jun. 1998.

[38] R. Smith, "Optical power handling capacity of low loss optical fibers as determined by stimulated Raman and Brillouin scattering," *Applied Optics*, vol. 11, no. 11, pp. 2489–2494, Nov. 1972.

[39] G. P. Agrawal, *Fiber Optic Communication Systems*, 2nd ed. New York: John Wiley & Sons, 1997.

[40] P. Wait and T. Newson, "Landau Placzek ratio applied to distributed fibre sensing," *Optics Communications*, vol. 122, pp. 141–146, Jan. 1996.

[41] J. Stone and A. Chraplyvy, "Spontanous Brillouin noise in long-distance high-bandwidth optical-fibre transmission," *Electronics Letters*, vol. 19, no. 8, pp. 275–277, Apr. 1983.

[42] R. Boyd, K. Rzazewski, and P. Narum, "Noise initiaton of stimulated Brillouin scattering," *Physical Review A*, vol. 42, no. 9, pp. 5514–5521, Nov. 1990.

[43] R. Feced, T. Parker, M. Farhadiroushan, V. Handerek, and A. Rogers, "Power measurement of noise-initiated Brillouin scattering in optical fibers for sensing applications," *Optics Letters*, vol. 23, no. 1, pp. 79–81, Jan. 1998.

[44] J. Jackson, *Classical Electrodynamics*, 2nd ed. New York: John Wiley & Sons, 1975.

[45] A. H. Hartog and M. P. Gold, "On the theory of backscattering in single-mode optical fibers," *Journal of Lightwave Technology*, vol. LT-2, no. 2, pp. 76–82, Apr. 1984.

[46] E. Snitzer, "Cylyndrical dielectric waveguide modes," *Journal of the Optical Society of America*, vol. 51, no. 5, pp. 491–498, May 1961.

[47] A. Snyder and J. Love, *Optical Waveguide Theory*. London: Chapman and Hall, 1983.

[48] A. Safaai-Jazi and G. Yip, "Scattering from an arbitrarily located off-axis inhomogeneity in a step-index optical fiber," *IEEE Transactions on Microwave Theory and Techniques*, vol. MTT-28, no. 1, pp. 24–32, Jan. 1980.

[49] ——, "Scattering from an off-axis inhomogeneity in step-index optical fibers: radiation loss," *Journal of The Optical Society of America*, vol. 70, no. 1, pp. 40–48, Jan. 1980.

[50] A. Snyder, "Scattering due to irregularities on dielectric or optical fibres," *Electronics Letters*, vol. 5, no. 12, pp. 271–272, Jun. 1969.

[51] K. Saito, M. Yamaguchi, and A. J. Ikushima, "Approach for reducing the Rayleigh scattering loss in optical fibers," *Journal of Aapplied Physics*, vol. 95, no. 4, pp. 1733–1735, Feb. 2004.

[52] Corning Incorporated, "Corning SMF-28 fiber product information," NY: Corning, Inc., 2001.

APPENDIX A

CHARACTERISTICS OF THE SMF-28 FIBER

The information provided here has been taken from the product information booklet provided by Corning [52]. All the values are at 1550 nm wavelength unless stated otherwise.

Table I. Characteristics of the SMF28 single mode fiber

Characteristic	Typical Symbol	Value [Units]
Effective Group Index of Refraction	N_{eff}	1.4682
Rayleigh Backscatter Coefficient (for 1 ns pulse width)		-82 dB
Core Diameter		8.2 μm
Cladding Diameter		125.0 $\pm$ 1.0 μm
Numerical Aperture	NA	0.14
Mode-Field Diameter		10.4 $\pm$.8 μm
Typical Attenuation		0.19 dB/km

APPENDIX B

PROGRAM CODES

```
/*****************************************************************/
// Main program. Filename: OTDRs.cpp
// Aleksander Wojcik
/*****************************************************************/

#include "custom.h"

const double c=299792458;
const double pi=3.1415926535898;

void main(void)
{
MotherOfAll urng;    // declare uniform random number generator
Random::Set(urng);   // set urng as generator to be used

Uniform U;
fstream fout,foutc;
char filename[]="output.txt";
char controlf[]="control.txt";

int control;
```

```
double p;
double L;
double k;

complejo c1(0.0,1.0),c2(0.0,1.0);
int jj,kk,DATA,M;
int N,per;
complejo *E;
complejo *G;
double posi;
double Tp;
double pos;

complejo T;
complejo H;

stringstream out_filename;
string of;

// Parameters

DATA=20000;    // Number of simulations
k=1000;        // wavenumber
M=1000;         // number of scatterers
p=0.5;
Tp=pi/2.0;
```

```
L=100;

control=0;     // 1 for control.txt file, 0 to supress
                              // control file just generates number
                              //of perturbed scatterers in %

// End of Parameters

E=new complejo[M];
G=new complejo[M];
per=floor(DATA/100);
N=floor(M*p);



out_filename << "p" << p << "_Tp" << Tp;
out_filename << << "_M" << M << "_D" << DATA/1000;
out_filename << "k_" << filename;

of = out_filename.str();

fout.open(of.c_str(),ios::out);
if(control==1)
    foutc.open(controlf,ios::out);

cout << "\n Starting Monte Carlo Simulation. \n\n";
```

```
for(kk=0;kk<DATA;kk++)
{

    if(kk%per==0)
        cout << "Progress " << 100*(kk+1)/DATA << " %\n";

    posi=0;

    for(jj=0;jj<M;jj++)
    {
        pos=U.Next();

        E[jj]=exp(_j*k*pos*L);
        G[jj]=E[jj];
        if(pos>p)
        {
            G[jj]=G[jj]*exp(_j*Tp);
        posi++;
        }
    }

    T=_z;
    H=_z;

    for(jj=0;jj<M;jj++)
    {
```

```
        T=T+E[jj];
        H=H+G[jj];
    }
    fout << abs(T)*abs(T) << "\t" << abs(H)*abs(H) << "\n";
    if(control==1)
        foutc << 100*(posi/M) << "\n";
}

fout.close();
if(control==1)
    foutc.close();

cout << "\n\n Completed 100% \n";
cout << " Number of scatterers: " << M << "\n";
cout << " Number of simulations: " << DATA << "\n";
cout << " Perturbation in Radians: " << Tp << "\n";
cout << " Perturbation position (normalized): " << p << "\n";
cout << " Output file: " << out_filename.str() << "\n";

delete [] E;
delete [] G;

}

/*****************************************************************/
// Header File. Filename: custom.h
```

```
// Aleksander Wojcik
/*****************************************************************/

#include <iostream>
#include <fstream>
#include <complex>
#include <vector>
#include <sstream>
#include <string>

using namespace std;
#include "newran.h"

typedef complex<double> complejo;  // define complejo
typedef vector<complejo> vectorc; // vector of complex numbers


ostream& operator << (ostream& s, complejo& c)
{
    s << "(" << c.real() << "," << c.imag() << ")";
    return s;
}

template <class T>
ostream& operator << (ostream& s,vector<T>& v)
{
```

```
    int i;
    for(i=0;i<v.size();i++)
        s << v[i] << "\n";
    return s;
}



template <class T>
vector<T>& operator * (vector<T>& v,T& r)
{

    int i;
    for(i=0;i<v.size();i++)
        v[i]=v[i]*r;
    return v;
}

complejo _j(0.0,1.0);
complejo _z(0.0,0.0);
```

VITA

Aleksander Wójcik was born in Warsaw, Poland. He is the son of Dr. Aleksander Wójcik, statistics professor and Jadwiga Wójcik, economist. At the age of eleven, he and his family moved to Mexico. He started his undergraduate studies at ITESM, Campus Toluca, and two years later transferred to ITESM, Campus Monterrey. He graduated in December of 1999 with the degree of Bachelor in electrical engineering. In 2000, he started working at the Institute of Electrical Investigations in Cuernavaca, Mexico, in the department of Geothermy. In August of the same year he started his studies in the Microwave and Electromagnetics Laboratory at Texas A&M University, in College Station, Texas. He received his Master of Engineering in electrical engineering diploma in May of 2003. In August of 2003 he joined the Optics and Solid State Laboratory of the same university, and received a Ph.D in electrical engineering in December of 2006.

Mailing Address: Dr. Antonio Hernandez # 119 Casa 18, Toluca, Edo.de Mex., Mexico